Hindawi
Structural Control and Health Monitoring
Volume 2023, Article ID 4009397, 26 pages
https://doi.org/10.1155/2023/4009397

Research Article

Multiobjective Reliability-Based Design Optimization of the Fuzzy Logic Controller for MR Damper-Based Structures

Pei Pei,[1,2,3] **Ser Tong Quek**,[3] **and Yongbo Peng**[1,4]

[1]*State Key Laboratory of Disaster Reduction in Civil Engineering, Tongji University, Shanghai 200092, China*
[2]*College of Civil Engineering, Tongji University, Shanghai 200092, China*
[3]*Department of Civil and Environmental Engineering, National University of Singapore, 1 Engineering Drive 2, Singapore 117576, Singapore*
[4]*Shanghai Institute of Disaster Prevention and Relief, Tongji University, Shanghai 200092, China*

Correspondence should be addressed to Yongbo Peng; pengyongbo@tongji.edu.cn

Received 22 September 2022; Revised 31 January 2023; Accepted 29 May 2023; Published 14 August 2023

Academic Editor: Zoran Rakicevic

To devise an optimum and robust fuzzy logic controller for MR damper-based structures subjected to earthquake ground motions, the multiobjective reliability-based design optimization (RBDO) using the adaptive Kriging model is performed to determine the parameters of the fuzzy logic controller. The optimization problem is formulated with two objective functions, namely, the minimization of interstory drift and average control force of the concerned structure, and subjected to a probability constraint on structural dynamic responses under the effects of random structural stiffness and stochastic earthquake loadings. To reduce the computational cost of reliability assessment, a global Kriging model is constructed in an augmented space as a surrogate for computational evaluations. Subsequently, the trained metamodel combined with the nondominated sorting genetic algorithm (NSGA-II) is integrated into the framework of RBDO for solving the fuzzy logic control (FLC) optimization problem. The feasibility and effectiveness of the multiobjective RBDO in the FLC design are finally validated by conducting numerical simulations on both linear and nonlinear structures. As demonstrated in the linear case, the fuzzy logic controllers obtained from the multiobjective RBDO show more robustness than those derived from the multiobjective deterministic design optimization (DDO). In the nonlinear case, using the multiobjective DDO to prelocate a coarse safety domain can significantly reduce the number of samples for training the metamodel and facilitate the implementation of the multiobjective RBDO; in addition, the controlled structural performance with a specified fuzzy logic controller can be further improved by considering MR damper distribution optimization.

1. Introduction

The mitigation of structural vibrations caused by dynamic loads, such as earthquakes and winds, is of major concern among the structural engineering community. In this regard, various methods have been proposed for maintaining the safety and serviceability of civil engineering structures [1, 2]. Structural control has proved its value in protecting engineering structures against natural hazards [3–5]. In general, structural control can be classified into four categories, i.e., passive control, active control, hybrid control, and semiactive control [6]. Among these control modalities, semiactive control is most promising since it not only possesses the reliability of passive control systems and the adaptability of active control systems but also requires relatively much less external energy than the first three control systems [7–9]. A magnetorheological (MR) damper has been regarded as a promising fail-safe device for semiactive control of various structures, such as cable bridges [10, 11] and high-rise buildings [12, 13]. To utilize the full capacity of MR dampers, an effective and reliable control algorithm is always essential. Since 1996, various control algorithms have been successfully applied to MR damper-based structural systems, which can be grouped into model-based and nonmodel-based algorithms.

Representative model-based algorithms include the clipped-optimal algorithm [5, 14–18], modulated homogeneous friction algorithm [19], and decentralized bang-bang control algorithm [20]. They are generally composed of two controllers. One is the primary controller which is used to provide the reference control force, and the other is the secondary controller which produces the actual damping force dependent on the reference force. It is worth noting that the primary controller requires an accurate mathematical model to describe the dynamics of the controlled system. However, it is not always easy to build such an exact mathematical model, especially for some complicated structures.

Contrary to the model-based control algorithms mentioned above, the nonmodel-based algorithms, also known as intelligent control algorithms, can be used with little prior knowledge about structural dynamics; thus, they have drawn increasing attention from engineers and researchers. For instance, Xu et al. [21] developed an online real-time control scheme to provide semiactive control for the MR damper-based structure by training a four-layer feedforward neural network model. Hashemi et al. [22] constructed a wavelet neural network model for seismic semiactive control of a benchmark building, in which the model parameters were identified with a localized genetic algorithm (GA). Based on fuzzy set theory, Choi et al. [23] developed a semiactive fuzzy control algorithm for MR damper-based structural systems, and the parameters involved in this control scheme were defined based on human experience. Simulation results showed that this semiactive fuzzy control scheme was effective in reducing structural responses under a wide range of seismic excitation conditions. In fact, fuzzy logic control (FLC) is known for its insensitiveness to the uncertainties associated with the structural system, because it introduces human expertise into control strategy by using linguistic instructions. The latter has led to the FLC methodology being applied to many MR damper-based structural systems, such as base-isolated building structures [5], cable-stayed bridges [24], and offshore jacket platforms [25].

Although a fuzzy logic controller can be directly defined based on human experience or trial-and-error tests, many researchers have tried to identify the FLC parameters using optimization-based methods to obtain an optimal controller. For example, to reduce the seismic responses of a linear MR damper-based structure, Yan and Zhou [26] developed a fuzzy logic controller using GA to tune the fuzzy rules. In the optimization process, two optimization objectives, including minimizing both the maximum structural displacement and acceleration, were considered using the weighted multiobjective function. Aiming at the seismic mitigation of a 3-story benchmark building equipped with MR dampers, Shook et al. [27] optimized fuzzy logic controllers using a nondominated sorting genetic algorithm (NSGA-II), in which four objectives, i.e., minimizing the peak and root-mean-square (RMS) interstory drift and peak and RMS acceleration, were simultaneously considered. As a multiobjective optimization approach, NSGA-II generates a set of Pareto-optimal solutions instead of a single solution. An appropriate design for the specific performance requirement can then be conveniently selected from Pareto-optimal solutions. In this respect, NSGA-II has been widely applied to optimize the FLC-driven MR damper-based control system in various structures, such as base-isolated structures [28–30], adjacent buildings [31], torsion-responsive structures [32], and nonlinear and/or plan-asymmetric structures [33].

In the aforementioned literature review, the optimization works conducted on fuzzy logic controllers are all aimed at deterministic structural systems, the optimization objectives are mainly defined as the maximum or the average of structural responses, such as structural displacement and acceleration, and the performance of an optimized fuzzy logic controller is only verified by conducting numerical simulations on several selected scenarios. Actually, large uncertainties may exist in the MR damper-based structural system due to inherent randomness associated with structural properties and external loadings. These uncertainties may affect the reliability of the control system and even lead to unexpected structural failure. Therefore, the optimal design obtained from deterministic optimization design may be incomplete due to large uncertainties involved, and using only several parametric scenarios may not be sufficient to demonstrate the robustness of the fuzzy logic controller. It is claimed that FLC is characterized by its insensitiveness to uncertainties associated with the system, but this fact only stands in the premise of an optimal and robust fuzzy logic controller, which needs further investigation. In this respect, it is necessary to take the uncertainties into account in the design process of FLC to obtain an optimal and robust controller. To this end, reliability-based design optimization (RBDO), which seeks the optimal design with consideration of the parameter uncertainties and probability constraints, can provide a realistic and rational framework for designing a fuzzy logic controller. Furthermore, a more comprehensive assessment of the optimized fuzzy logic controller can then be performed.

Generally, an RBDO problem can be directly solved using the traditional two-level approach, in which the inner loop deals with reliability assessment and the outer loop deals with cost optimization. However, the two-level approach can be expensive in terms of model evaluations, especially for real-world optimization problems which often need to be solved using high-fidelity computational models. To improve the efficiency of solving expensive RBDO problems, some simplified solution strategies, such as the mono-level and decoupled approaches [34–36], have been developed to separate the reliability analysis loop from the optimization loop. However, these approaches still entail repeated function calls for reliability assessment, which will be computationally formidable when high-fidelity computational models are involved. In recent years, surrogate models, such as polynomial chaos expansion [37], support vector machine [38], radial basis function [39], and Kriging [40], have been widely used to replace the expensive-to-evaluate computational model and thus largely alleviated the computational burden of reliability assessment. Among these metamodels, Kriging has gained significant popularity, because it provides estimates of the expected model response

and the associated variance by interpreting the computational model as a realization of a Gaussian process. To save computational cost, some researchers have introduced the global modeling strategy associated with an adaptive updating scheme into RBDO [41], which tends to approximate the computational model over the entire domain of the random variable space.

The objective of this work is to develop an optimum and robust fuzzy logic controller for an MR damper-based structural system in the framework of RBDO. The approach taken is to combine the adaptive Kriging-based global modeling technique combined with NSGA-II to solve the RBDO problem. However, training a global surrogate model to accurately approximate the response of an FLC-driven structural system is not an easy task, because there are many design parameters involved in the FLC, and thus, a high-dimensional design space needs to be considered. By using control expertise, the fuzzy rule base can be conceptually predesigned with a significant reduction in the original design space. Subsequently, an augmented space is constructed by extending the narrowed design space with the space of random variables. Finally, the proposed RBDO problem can be readily solved using the double-loop strategy combined with NSGA-II and the Kriging model over the augmented space.

In what follows, Section 2 presents the problem formulation of optimizing fuzzy logic controllers for the MR damper based-structure whose parameters are modeled in a probabilistic framework. In Section 3, a multiobjective RBDO method is presented by combining the global Kriging model with NSGA-II to solve the optimization problem. Then, the optimization method is employed to optimize fuzzy logic controllers for both linear and nonlinear structural systems in Section 4. Finally, the findings are summarized in Section 5.

2. Problem Formulation

In this section, an FLC-driven MR damper-based structural system with consideration of random parameters in structural properties and external excitations is first constructed, and then, the optimization problem of FLC design is formulated in the framework of RBDO for mitigating the seismic response of the structure of interest.

2.1. Semiactive Structural Control System

2.1.1. Fuzzy Logic Control. FLC mainly uses a set of linguistic instructions based on human expertise to describe the relationship between input and output variables instead of complex mathematical expressions. A schematic view of the general architecture of FLC is depicted in Figure 1. As can be seen, there are four steps involved in the FLC design. The first step is fuzzification, in which the membership functions associated with each input variable are used to convert input crisp values to fuzzy linguistic values. In this paper, the structural acceleration and velocity are selected as two input variables, whose ranges are denoted as $[-r_1, r_1]$ and $[-r_2, r_2]$. r_1 and r_2 are set as 75% (usually 70%~80% in the literature [26, 42]) of the maximum interstory velocity and floor acceleration responses of the uncontrolled structure, respectively. The control force is chosen as the output variable, and its range, denoted as $[-r_3, r_3]$, will be determined in the subsequent optimization process.

Seven membership functions are defined for each input or output variable. As the Gaussian membership function can approximate almost all other types of membership functions, it is adopted herein for describing the central parts of input and output variables, as expressed by

$$\mu_G = e^{\left(-(x-b)^2/2a^2\right)}, \tag{1}$$

where a and b are the width and the central position of the Gaussian membership function, respectively. The two outermost parts of both input and output variables are, respectively, described by the spline-based Z-shaped and S-shaped membership functions:

$$\mu_Z = \begin{cases} 1, & x \le g, \\ 1 - 2\left(\dfrac{x-g}{h-g}\right)^2, & g \le x \le \dfrac{g+h}{2}, \\ 2\left(\dfrac{x-h}{h-g}\right)^2, & \dfrac{g+h}{2} \le x \le h, \\ 0, & x \ge h, \end{cases}$$

$$\mu_S = \begin{cases} 0, & x \le p, \\ 2\left(\dfrac{x-p}{q-p}\right)^2, & p \le x \le \dfrac{p+q}{2}, \\ 1 - 2\left(\dfrac{x-q}{q-p}\right)^2, & \dfrac{p+q}{2} \le x \le q, \\ 1, & x \ge q, \end{cases} \tag{2}$$

where g and h are the central position and the width of the Z-shaped membership function and q and p are the central position and the width of the S-shaped membership function. It is obvious that the configuration of input or output membership functions is determined by the aforementioned parameters, including a, b, g, h, p, and q. It is worth noting that g and q usually take the values of the lower and upper bounds of the input (or output) variable, i.e., r_i and r_i ($i = 1, 2, 3$). Therefore, only a, b, h, and p are undetermined, which are then normalized by their corresponding ranges and defined as the design variables. A set of evenly distributed membership functions are illustrated in Figure 2, as an example. As can be seen, each input or output has seven fuzzy linguistic variables, including negative large (NL), negative medium (NM), negative small (NS), zero (ZE), positive small (PS), positive medium (PM), and positive large (PL).

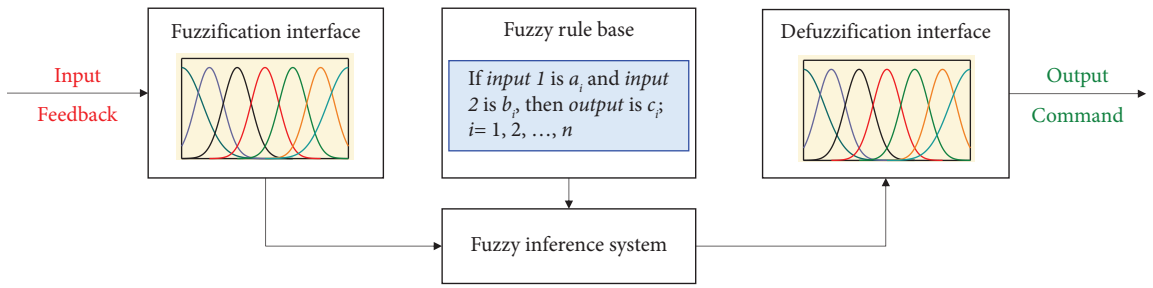

Figure 1: General architecture of FLC.

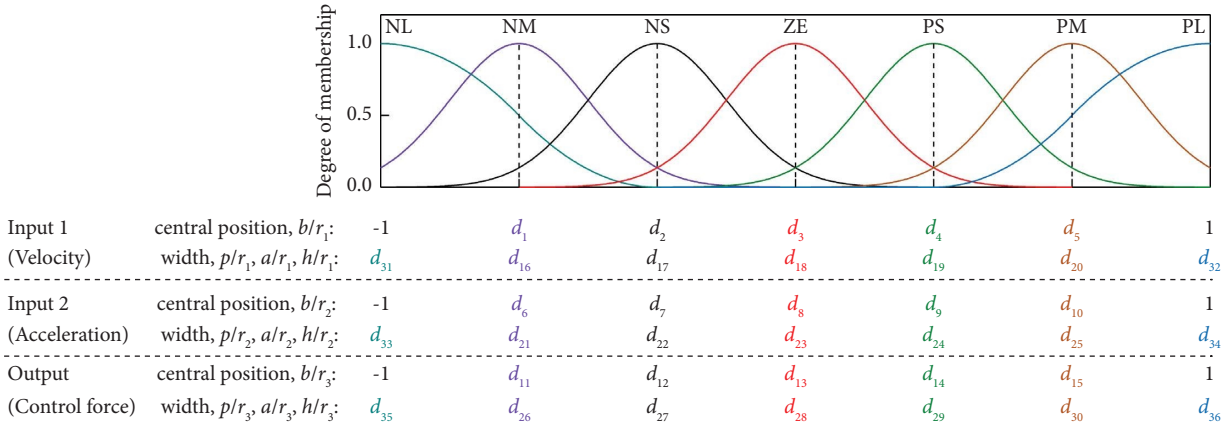

Figure 2: Evenly distributed membership functions of the input (or output) variable.

In the second step of fuzzy rule design, IF-THEN rules are employed for constructing the rule base of FLC. Since both Inputs 1 and 2 are represented by seven membership functions, $7 \times 7 = 49$ fuzzy rules need to be designed, as shown in Figure 3. For clarity, an example of the if-premise-then-consequent statement is expressed as follows: **if** input 1 (structural velocity) is NL and input 2 (structural acceleration) is NM, **then** output (control force) is NL.

The third step, i.e., fuzzy inference design, is the kernel of a fuzzy logic controller, which characterizes the transformation from input to output. In this study, the Mamdani-type inference engine is used [43].

As the last step of FLC, the defuzzification interface describes the mapping from the space of fuzzy outputs to the space of crisp outputs. Here, the center of gravity (CG) method is employed to transform the fuzzy output obtained from the fuzzy inference system into the crisp control output. For the j-th rule of the i-th input variables, the command force F_i calculated by the CG method is expressed by

$$F_i = \frac{\sum_{j=1}^{n_r} c_i^{(j)} \int \mu_i^{(j)}}{\sum_{j=1}^{n_r} \int \mu_i^{(j)}}, \tag{3}$$

where n_r represents the number of fuzzy rules, $\mu_i^{(j)}$ denotes the membership function corresponding to the output variable defined in the consequent statement of the j-th rule for the i-th input variable, and $c_i^{(j)}$ denotes the center of the membership function $\mu_i^{(j)}$.

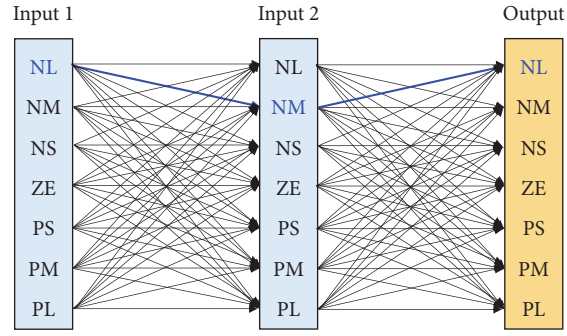

Figure 3: Schematic of fuzzy rules.

2.1.2. Inverse Modeling for Current Identification of the MR Damper. The MR damper is directly commanded by the input current instead of the control force provided by the constructed fuzzy logic controller. Therefore, an inverse dynamic model needs to be developed for identifying the input current according to the desired control force derived from the fuzzy logic controller. In this work, a simple inverse modeling technique proposed in [44] is used, which is developed based on a forward dynamic model of the MR damper, i.e., the modified Bingham-plastic model, as expressed by

$$F_{\mathrm{MR}} = kx + \lambda f_y + \xi f_h, \tag{4}$$

where F_{MR} is the damping force produced by the MR damper, x denotes the damper displacement, f_y and f_h are, respectively, the yielding and hysteretic forces, k is the spring

stiffness, and ξ and λ are, respectively, the hysteretic operator and the coefficient for controlling the low-velocity stress, defined as follows:

$$\xi = \arctan\left\{\frac{[\dot{x} - \dot{x}_H \mathrm{sgn}(x)]}{\dot{x}_a}\right\}, \tag{5}$$

$$\lambda = \frac{2}{\pi}\mathrm{sgn}(\dot{x})\arctan\left(\left|\frac{\dot{x}}{\dot{x}_b}\right|\right), \tag{6}$$

where $\dot{x}$ denotes the damper velocity, $\dot{x}_a$ and $\dot{x}_b$ are two different reference velocities for the nondimensional purpose, and $\dot{x}_H$ is the hysteretic velocity. The model parameters in equations (4)–(6) are then identified to correlate with the input current I through fitting the experimental data using the polynomial function [45], as listed in Table 1.

Based on the forward dynamic model presented above, the inverse modeling technique is then developed, which updates the input current by analyzing the damper motion state and calculating the damper force until the desired control force at the present instant of time is obtained. For clarity, the detailed computational procedure is presented in Algorithm 1, where i denotes the present instant of time.

2.1.3. Structural Model. By combining the fuzzy logic controller and MR damper, a semiactive structural control system is constructed, which is investigated as an n-degree of freedom lumped mass system here. The corresponding dynamic model is shown in Figure 4(a), and the equation of motion is formulated as follows:

$$\begin{aligned}\mathbf{M}(\Theta)\ddot{\mathbf{U}}(t) + \mathbf{C}(\Theta)\dot{\mathbf{U}}(t) + \mathbf{f}(\mathbf{U}, \dot{\mathbf{U}}(t), \Theta)\\ = \mathbf{B}\mathbf{F}_d(\Theta, t) - \mathbf{M}\mathbf{I}_e\ddot{u}_g(\Theta, t),\end{aligned} \tag{7}$$

where $\mathbf{U}$ represents the vector of structural displacement relative to the ground, "." and ".." above $\mathbf{U}$ denote the vectors of velocity and acceleration relative to the ground, $\mathbf{M}$, $\mathbf{C}$, and $\mathbf{f}$ are the mass matrix, damping matrix, and restoring force vector, respectively, $\mathbf{F}_d$ is the force vector containing control forces provided by the MR damper, $\mathbf{B}$ is the matrix denoting the damper location, $\boldsymbol{\Theta}$ represents the vector of random parameters (environmental variables) involved in structural properties and external excitations, $\mathbf{I}_e$ denotes the unit vector of size n, and $\ddot{u}_{\mathbf{g}}(\Theta, t)$ denotes the ground motion excitation and is assumed as follows:

$$\ddot{u}_{\mathbf{g}}(\Theta, t) = \left(\theta_1\ddot{u}_{g1}(t) + \theta_2\ddot{u}_{g2}(t)\right)\zeta, \tag{8}$$

where $\ddot{u}_{g1}(t)$ and $\ddot{u}_{g2}(t)$ represent the normalized El Centro acceleration records in the N-S and E-W directions, as shown in Figure 4(b), θ_1 and θ_2 are the corresponding stochastic coefficients, and ζ is the amplitude coefficient.

2.2. Problem Formulation. To strengthen and improve the constructed semiactive structural control system, an optimum and robust fuzzy logic controller needs to be properly designed. From the perspectives of both safety and economy, the minimization of maximum interstory drift as well as the minimization of average control force is selected as the objective function. According to Section 2.1.1, a total of $N_d = 86$ parameters involved in the input and output membership functions and rule base are undetermined and thus defined as the design variable, of which d_1~d_5 and d_{16}~d_{20}, respectively, represent the central positions and widths of Gaussian membership functions in input 1, d_6~d_{10} and d_{21}~d_{25}, respectively, represent the central positions and widths of Gaussian membership functions in input 2, d_{11}~d_{15} and d_{26}~d_{30}, respectively, represent the central positions and widths of Gaussian membership functions in output, d_{31}, and d_{32}, respectively, represent the widths of Z- and S-shaped membership functions in input 1, d_{33} and d_{34}, respectively, represent the widths of Z- and S-shaped membership functions in input 2, d_{35} and d_{36}, respectively, represent the widths of Z- and S-shaped membership functions in output, d_{37} represents the range of output variable, and d_{38}~d_{86} represent the fuzzy rules. Here, some soft constraints need to be defined to regulate the range of these design variables. A first, the range of output variable d_{37} is defined. It is worth mentioning that a too small output range may restrict the optimization space of the membership function, while a too broad range will increase the computing cost. In this respect, a relatively appropriate output range (see equation (9)) is defined here to ensure that the output control force is within a reasonable range as well as to provide more possibility to search for an optimum solution to the membership functions without increasing too much computing cost:

$$\frac{1}{2}F_{\mathrm{MR,max}} \le d_{37} \le 2F_{\mathrm{MR,max}}, \tag{9}$$

where $F_{\mathrm{MR,max}}$ is the maximum damping capacity of the MR damper.

If the movements of the fuzzy sets are left unconstrained, the resulting system may have linguistically meaningless sets. This evolution will alter the predetermined initial rule. Consistently, the new erroneous rule will have a great effect on the performance of the control system. Therefore, it is necessary to impose a set of inequality constraints for the membership functions, which can not only prevent this failure but also help minimize the computational cost associated with the membership function optimization. In some FLC-related optimization works [46, 47], these constraints have been adopted directly or indirectly. Therefore, second, the initial order of the central positions of fuzzy sets needs to be maintained by setting the following constraints:

$$-1 \le d_1 \le d_2 \le d_3 \le d_4 \le d_5 \le 1, \tag{10}$$

$$-1 \le d_6 \le d_7 \le d_8 \le d_9 \le d_{10} \le 1, \tag{11}$$

$$-1 \le d_{11} \le d_{12} \le d_{13} \le d_{14} \le d_{15} \le 1. \tag{12}$$

Third, if the width of membership functions is too large, the system sensitivity will be decreased; in contrast, if the width of membership functions is too small, the system stability will be decreased. Therefore, without loss of generality, the following restrictions covering a wide range of possibilities are given:

Table 1: Fitting equations of current-dependent parameters.

Parameters type	Fitting equation
Force-related parameters	$k = -0.2997I^3 + 1.9563I^2 - 3.7818I - 0.236$
	$f_h = 5.101I^3 - 50.197I^2 + 131.56I + 4.0539$
	$f_y = -45.090I^3 + 152.930I^2 - 147.940I + 76.710$
Displacement-related parameters	$\dot{x}_H = -0.1209I^3 + 0.8308I^2 - 1.7046I - 0.5106$
	$\dot{x}_a = -0.1347I^4 + 0.6602I^3 - 1.0982I^2 + 0.7768I + 0.204$
	$\dot{x}_b = -12.786I^4 + 61.726I^3 - 105.4I^2 + 76.802I - 23.489$

(1) **Input:** state variable, desired control force $F_{de,i}$.
(2) Define initial input current $I_i = 0$, force error $F_{\epsilon,i} = 1$, and $j = 1$.
(3) **While** $F_{\epsilon,i} \leq 10^{-6}$
(4) Update input current, $I_i = I_i + j \times 0.1$.
(5) Calculate current-dependent parameters ξ_i, λ_i, and k_i, see Table 1.
(6) Calculate damper force $F_{MR,i}$ using equation (4).
(7) $F_{\epsilon,i} = F_{de,i} - F_{MR,i}$
(8) **If** any of the following cases holds, **break**.
(1) $F_{MR,i} < 0$, $F_{de,i} > 0$, $\xi_i < 0$, $\lambda_i < 0$, $x_i > 0$
(2) $F_{MR,i} > 0$, $F_{de,i} < 0$, $\xi_i > 0$, $\lambda_i > 0$, $x_i < 0$
(3) $F_{MR,i} < 0$, $F_{de,i} < 0$, $F_{\epsilon,i} > 0$, $\xi_i > 0$, $\lambda_i > 0$, $x_i < 0$
(4) $F_{MR,i} > 0$, $F_{de,i} > 0$, $F_{\epsilon,i} < 0$, $\xi_i < 0$, $\lambda_i < 0$, $x_i > 0$
(9) **End if**
(10) $j = j + 1$
(11) **Return:** I_i

Algorithm 1: Implementation procedure of the inverse modeling technique.

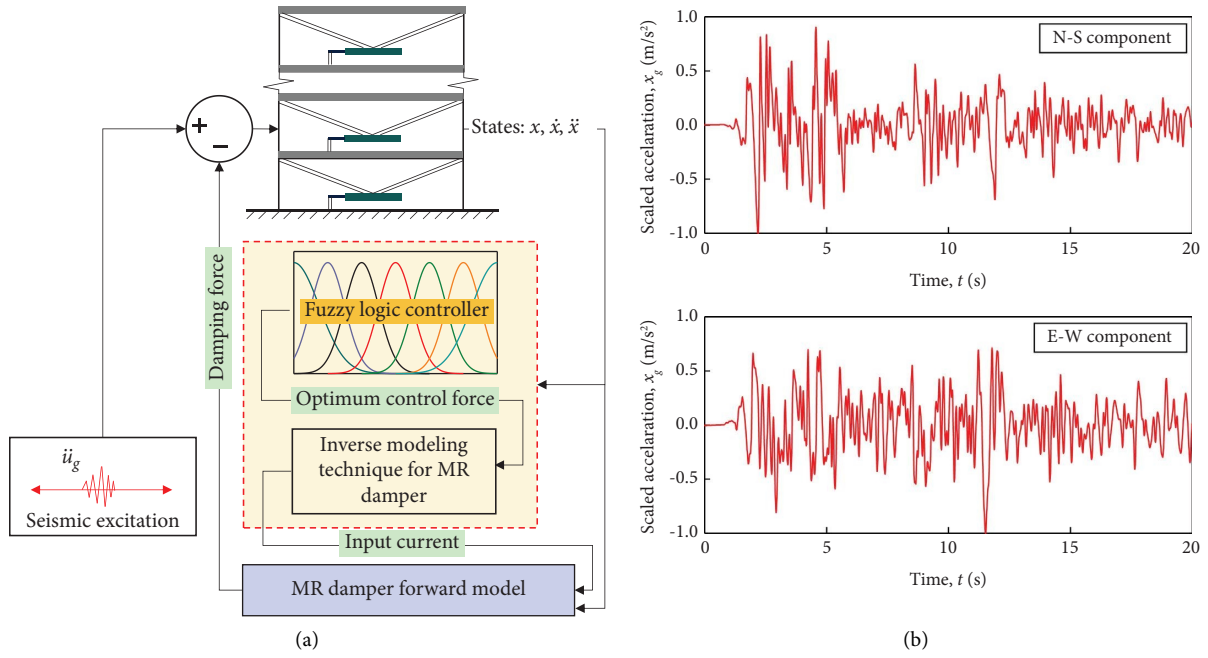

Figure 4: Schematic of the FLC-driven MR-damper-based structural system and input seismic excitations. (a) Dynamic model of the MR damper-based structure. (b) El Centro accelerogram in orthogonal directions.

$$0.1 \le d_i \le 2.0, \quad (i = 16, \ldots, 30), \tag{13}$$

$$-\frac{5}{6} \le d_i \le \frac{3}{6}, \quad (i = 31, \ldots, 36). \tag{14}$$

For clarity, Figure 5 has illustrated the width ranges of Z-shaped, S-shaped, and Gaussian membership functions defined in equations (13) and (14). As can be seen, a broad range of width can be covered with consideration of the constraints given in equations (13) and (14).

On the other hand, two hard constraints are also considered here. The first one is the probability constraint, which has considered the uncertainties involved in structural properties and external excitations. The constructed semiactive control system is assumed to be failed when the maximum interstory drift across all stories exceeds a prescribed threshold u_{thr}. The corresponding failure probability of the concerned structural system is thus given by

$$P_f = \Pr\{Y_{\text{EEV}} \ge u_{\text{thr}}\}, \tag{15}$$

where Y_{EEV} denotes the equivalent extreme value (EEV) of interstory drift, defined as follows:

$$Y_{\text{EEV}} = \max_{1 \le j \le n_f} \left\{ \max_{0 \le t \le T} \left(U_{\text{in},j}(\Theta, t) \right) \right\}, \tag{16}$$

where $U_{\text{in},j}(\boldsymbol{\Theta}, t)$ is the interstory drift of j-th floor at time t, n_f is the number of structure floors, and $[0, T]$ corresponds to the time duration. The other hard constraint is that the maximum control force should not exceed the maximum damping capacity $F_{\max}$ of the MR damper.

Based on the abovementioned statements, the RBDO problem for the constructed semiactive structural control system is finally formulated, as shown in equation (17). In this formulation, two objectives are considered, in which the minimization of average control force is to save control cost and the minimization of maximum interstory drift is to reduce the earthquake-induced structural responses. It is noted that the hard constraint regarding failure probability can also help reduce the interstory drift in the optimization process, but it only ensures that the probability of the maximum interstory drift exceeding the defined threshold is lower than the target failure probability. However, the defined threshold is usually given based on the existing design codes and is not a small value. Therefore, there is still a lot of room for further reducing the structural responses when the hard constraint is satisfied. In this respect, two competing objective functions are defined, in an attempt to explore fuzzy logic controllers with high performance and low control cost:

$$\begin{aligned} &\text{find } \mathbf{d} = [d_1, d_2, \ldots, d_{86}], \\ &\min \ \mathbf{c} = [S_{\max}(\mathbf{d}), F_{\text{ave}}(\mathbf{d})], \\ &\text{s.t.} \begin{cases} \text{hard constraint: } \mathbb{P}[g(\mathbf{d}, \mathbf{E}) \le 0] \le P_{f0}, \\ \max(\mathbf{F}_{\text{con}}(\mathbf{d})) \le F_{\max}, \\ \text{soft constraint: } f_j(\mathbf{d}) \le 0, \quad \{j = 1, \ldots, n_s\}, \end{cases} \end{aligned} \tag{17}$$

where $\mathbf{d}$ represents the vector of design variables, $\mathbf{E}$ denotes the vector of random environmental variables, $\mathbf{c}$ is the vector of the objective function, including the maximum interstory drift $S_{\max}(\mathbf{d})$ and the average control force $F_{\text{ave}}(\mathbf{d})$, $\Pi(\cdot)$ represents the probability measure of a random event, $g(\cdot)$ represents the limit state function (LSF), $\mathbf{F}_{\text{con}}(\cdot)$ represents the actual control force generated by the MR damper, $P_{f0} = 10^{-3}$ denotes the target failure probability, and $f_j(\mathbf{d})$ represents the soft constraints defined in equations (9)–(14).

3. Multiobjective Reliability-Based Design Optimization Using Adaptive Kriging

To solve the RBDO problem formulated in Section 2, an augmented space is constructed by combining the design and environmental space, and a global adaptive Kriging surrogate is then constructed in the augmented space. This is finally combined with NSGA-II to solve the optimization problem with consideration of two objectives. A brief review of the Kriging metamodel is given first as follows.

3.1. Kriging Model. To save the computational cost caused by the reliability assessment, metamodels are usually employed to approximate the limit-state functions in RBDO. In this work, the Kriging model $\mathscr{M}^{(K)}(\mathbf{x})$ is applied to surrogate the time-consuming computational model $\mathscr{M}(\mathbf{x})$ of the structural system of interest. In universal Kriging, the computational model $\mathscr{M}(\mathbf{x})$ is interpreted as a realization of an underlying Gaussian process:

$$\mathscr{M}(\mathbf{x}) \approx \mathscr{M}^{(K)}(\mathbf{x}) = \boldsymbol{\beta}^{\mathrm{T}} \cdot \mathbf{f}(\mathbf{x}) + \sigma^2 Z(\mathbf{x}), \tag{18}$$

where $\boldsymbol{\beta}^T \cdot \mathbf{f}(\mathbf{x})$ represents the trend given by the mean value of the Gaussian process, consisting of P arbitrary functions $\{f_j; j = 1, \ldots, P\}$ and the corresponding coefficients $\{\beta_j; j = 1, \ldots, P\}$. In this paper, the ordinary Kriging model is employed, in which $\mathbf{f}(\mathbf{x}) = 1$ and β is an unknown constant, as has been widely utilized [48–50]. σ^2 denotes the variance of the Gaussian process, $Z(\mathbf{x})$ represents a zero mean, unit variance, stationary Gaussian process, and the autocovariance of samples x_k, and x_k' is described using the Matérn-3/2 correlation function [51]:

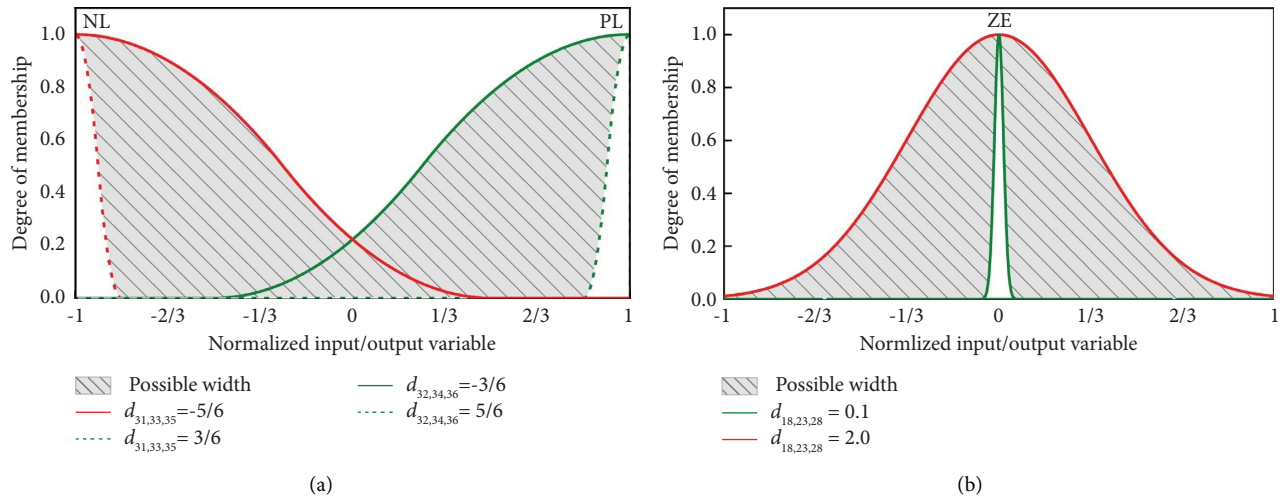

Figure 5: Width range of membership functions: (a) Z- and S-shaped membership functions; (b) Gaussian membership functions.

$$R_{M3/2}\left(\mathbf{x},\mathbf{x}';\boldsymbol{\theta}\right)=\prod_{k=1}^{N_k}\left(1+\sqrt{3}\ \frac{\left|x_k-x_k'\right|}{\theta_k}\right)\exp\left[-\sqrt{3}\ \frac{\left|x_k-x_k'\right|}{\theta_k}\right], \tag{19}$$

where $\boldsymbol{\theta}=\{\theta_k>0,k=1,\ldots,N_t\}$ are hyperparameters and N_t is the number of dimensions.

We consider a training dataset $\mathscr{W}=\{\mathscr{X},\mathscr{Y}\}$ consisting of the experimental design $\mathscr{X}=\{\mathbf{x}^{(1)},\ldots,\mathbf{x}^{(N)}\}$ and the corresponding computational model evaluations $\mathscr{Y}=\left\{y_{\mathrm{EEV}}^{(1)}=\mathscr{M}(\mathbf{x}^{(1)}),\ldots,y_{\mathrm{EEV}}^{(N)}=\mathscr{M}(\mathbf{x}^{(N)})\right\}$, and $\boldsymbol{\beta}$ and σ^2 are, respectively, estimated by

$$\begin{aligned}\hat{\boldsymbol{\beta}}(\boldsymbol{\theta})&=\left(\mathbf{1}^T\mathbf{R}_{\boldsymbol{\theta}}^{-1}\mathbf{1}\right)^{-1}\mathbf{1}^T\mathbf{R}_{\boldsymbol{\theta}}^{-1}\mathscr{Y},\\ \hat{\sigma}^2(\boldsymbol{\theta})&=\frac{1}{N}\left(\mathscr{Y}-\mathbf{1}^T\hat{\boldsymbol{\beta}}(\boldsymbol{\theta})\right)^T\mathbf{R}_{\boldsymbol{\theta}}^{-1}\left(\mathscr{Y}-\mathbf{1}^T\hat{\boldsymbol{\beta}}(\boldsymbol{\theta})\right),\end{aligned} \tag{20}$$

where $\mathbf{R}$ is the correlation matrix with elements $R_{\boldsymbol{\theta}}^{(i,j)}=R_{M3/2}(\mathbf{x}^{(i)},\mathbf{x}^{(j)};\boldsymbol{\theta}),i,j=1,\ldots,N$. Clearly, both $\hat{\boldsymbol{\beta}}$ and $\hat{\sigma}^2$ depend on $\boldsymbol{\theta}$ through the correlation matrix $\mathbf{R}_{M3/2}$. Then, $\boldsymbol{\theta}$ can be estimated by

$$\hat{\boldsymbol{\theta}}=\underset{\boldsymbol{\theta}}{\operatorname{argmin}}\left(\hat{\sigma}^2(\boldsymbol{\theta})\left(\det\left(R_{M3/2}(\boldsymbol{\theta})\right)\right)^{1/N}\right), \tag{21}$$

where $\det(\cdot)$ is the determinant operator. The Kriging prediction at an unknown point $\mathbf{x}$ follows Gaussian distribution, that is $\mathscr{M}^{(K)}(\mathbf{x})\sim\mathscr{N}(\mu_{\hat{y}}(\mathbf{x}),\sigma_{\hat{y}}(\mathbf{x}))$, with the mean $\mu_{\hat{y}}(\mathbf{x})$ and the variance $\sigma_{\hat{y}}(\mathbf{x})$ given by

$$\begin{aligned}\mu_{\hat{y}}(\mathbf{x})&=\mathbf{f}(\mathbf{x})^T\hat{\boldsymbol{\beta}}+\mathbf{r}(\mathbf{x})^T\mathbf{R}^{-1}(\mathscr{Y}-\mathbf{F}\hat{\boldsymbol{\beta}}),\\ \sigma_{\hat{y}}(\mathbf{x})&=\hat{\sigma}^2\left(1-\mathbf{r}(\mathbf{x})^T\mathbf{R}^{-1}\mathbf{r}(\mathbf{x})^T+\mathbf{u}(\mathbf{x})^T\left(\mathbf{F}^T\mathbf{R}^{-1}\mathbf{F}\right)^{-1}\mathbf{u}(\mathbf{x})\right),\end{aligned} \tag{22}$$

in which $\mathbf{r}(\mathbf{x})=[\mathbf{R}_{M3/2}(\mathbf{x},\mathbf{x}^{(1)}),\ldots,\mathbf{R}_{M3/2}(\mathbf{x},\mathbf{x}^{(N)})]^T$ and $\mathbf{u}(\mathbf{x})=\mathbf{F}^T\mathbf{R}_{M3/2}^{-1}\mathbf{r}(\mathbf{x})-\mathbf{f}(\mathbf{x})$.

3.2. Augmented Space. The surrogate model can provide a cheap approximation to the expensive-to-evaluate limit extreme state function of a complex structural system, especially when repeated evaluations are needed. This problem becomes more prominent when solving RBDO problems using the local modeling strategy, where the surrogate model needs to be repeatedly updated for each reliability assessment. As a comparison, the global modeling strategy offers a more efficient approach, in which a single surrogate model is built to approximate the whole constraint boundary in an augmented space [41, 52, 53]. The RBDO process can then proceed to search for the optimal solution using the constructed model. Therefore, in the following subsections, an augmented design space is established based on the space of design and environmental variables. To further improve the computational efficiency, the original design space is first narrowed down by regulating the range of design variables as well as predesigning the fuzzy rules based on control expertise.

3.2.1. Reduced Design Space. For constructing the augmented space, the design parameters are assumed to be uniformly distributed in this work. It is noted that there exist inequality relationships between some design parameters, see equations (10)–(12). Then, these parameters are dependent on each other, which will complicate the problem. Actually, most RBDO-related studies have been reported for tackling problems where design parameters follow independent probability distributions. In this respect, for simplification, a determined and equal range is allocated to each design parameter involved in equations (10)–(12) to

avoid introducing inequality constraints among parameters, as expressed by

$$\begin{aligned}
&-\frac{5}{6} \le d_1 \le -\frac{3}{6}, -\frac{3}{6} \le d_2 \le -\frac{1}{6}, -\frac{1}{6} \le d_3 \le \frac{1}{6}, \frac{1}{6} \le d_4 \le \frac{3}{6}, \frac{3}{6} \le d_5 \le \frac{5}{6},\\
&-\frac{5}{6} \le d_6 \le -\frac{3}{6}, -\frac{3}{6} \le d_7 \le -\frac{1}{6}, -\frac{1}{6} \le d_8 \le \frac{1}{6}, \frac{1}{6} \le d_9 \le \frac{3}{6}, \frac{3}{6} \le d_{10} \le \frac{5}{6},\\
&-\frac{5}{6} \le d_{11} \le -\frac{3}{6}, -\frac{3}{6} \le d_{12} \le -\frac{1}{6}, -\frac{1}{6} \le d_{13} \le \frac{1}{6}, \frac{1}{6} \le d_{14} \le \frac{3}{6}, \frac{3}{6} \le d_{15} \le \frac{5}{6}.
\end{aligned} \tag{23}$$

To further narrow down the design space, the fuzzy rules are designed here by incorporating human expertise into linguistic IF-THEN rules. It is necessary to observe the structural movement states and understand the system dynamics for designing an appropriate rule base for a fuzzy logic controller. Sinusoidal excitation-based testing or experiment is the most traditional method for testing or exploring the motion law of structures [54]. Therefore, for simplicity, a sinusoidal movement is assumed, and the corresponding structural states, including displacement, velocity, and acceleration are illustrated in Figure 6 [44].

As observed, one may find distinct characteristics of the structural motion states, which can be summarized as follows:

State 1: The structural acceleration and velocity are both positive (or negative), and the absolute value of the former is increasing, while the latter is decreasing; in the meantime, the structural displacement is increasing, indicating the structure is deviating from the central position. Therefore, a large control force is demanded for suppressing the structural motion.

State 2: The structural acceleration and velocity are opposite in sign, and the absolute value of the former is decreasing, while the latter is increasing; in the meantime, the structural displacement shows a decreasing trend, indicating the structure is getting back to the central position. In this case, the control force can be arranged at a small or zero value.

According to the two states summarized above, the structural motion can be regarded as symmetrical behavior, and thus, a standard symmetric rule base is devised here. A detailed description is given in Table 2. Consequently, with the predesigned fuzzy rules (where 49 parameters are defined), only the parameters involved in the input and output membership functions need to be optimized. The number of design variables N_d has decreased from 86 to 37, and the design space has been largely narrowed down.

3.2.2. Augmented Space. The augmented design space built here is the tensor product of confidence regions defined for the design and environmental variables, i.e., $\Delta = \Xi \times E$, where Ξ refers to the space of design variables and E is the space of environmental parameters [41]. Therefore, the bounds of the associated augmented space in the i-th dimension are defined as

$$\begin{aligned}
x_i^- &= F^{-1}_{X_i|d_i^-}\left(\frac{\alpha_{d_i}}{2}\right),\\
x_i^+ &= F^{-1}_{X_i|d_i^+}\left(1-\frac{\alpha_{d_i}}{2}\right),
\end{aligned} \tag{24}$$

where d_i denotes the i-th design parameter with lower and upper bounds of d_i^- and d_i^+, X_i follows the marginal distribution, $F^{-1}_{X_i|d_i^-}$ and $F^{-1}_{X_i|d_i^+}$ are the corresponding inverse cumulative distribution functions (CDF), and α_{d_i} is the probability of sampling outside the augmented space in the i-th dimension. The design confidence region is eventually obtained by the following tensorization:

$$X = \prod_{i=1}^{N_d} [x_i^-, x_i^+]. \tag{25}$$

Similar to the design variables, the lower and upper bounds of the augmented space for environmental variables in the i-th dimension are defined as

$$\begin{aligned}
z_j^- &= F^{-1}_{Z_j}\left(\frac{\alpha_{z_j}}{2}\right),\\
z_j^+ &= F^{-1}_{Z_j}\left(\frac{1-\alpha_{z_j}}{2}\right),
\end{aligned} \tag{26}$$

where $F^{-1}_{Z_i}$ is the inverse CDF associated with the environmental variable Z_i and α_{z_i} is the probability of sampling outside the augmented space in the i-th dimension. Then, the associated confidence region can be obtained:

$$Z = \prod_{j=1}^{N_e} \left[z_j^-, z_j^+\right], \tag{27}$$

where N_e is the number of environmental variables. For clarity, Figure 7 illustrates an augmented space for a simple three-dimensional problem, which consists of one environmental and two design variables.

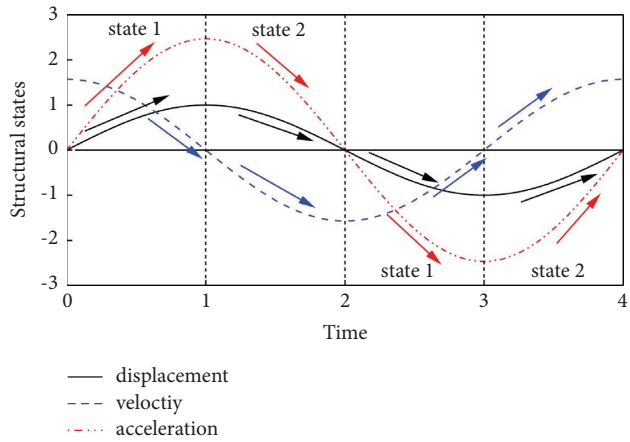

Figure 6: Structural motion states under sinusoidal movement.

Table 2: Predesigned fuzzy rules.

Acceleration	Velocity						
	NL	NM	NS	ZE	PS	PM	PL
NL	PL	PL	PM	PM	PS	NS	NS
NM	PL	PL	PM	PS	ZE	NS	NM
NS	PL	PL	PS	PS	ZE	NM	NM
ZE	PL	PM	PS	ZE	NS	NM	NL
PS	PM	PM	ZE	NS	NS	NL	NL
PM	PM	PS	ZE	NS	NM	NL	NL
PL	PM	PS	NS	NM	NM	NL	NL

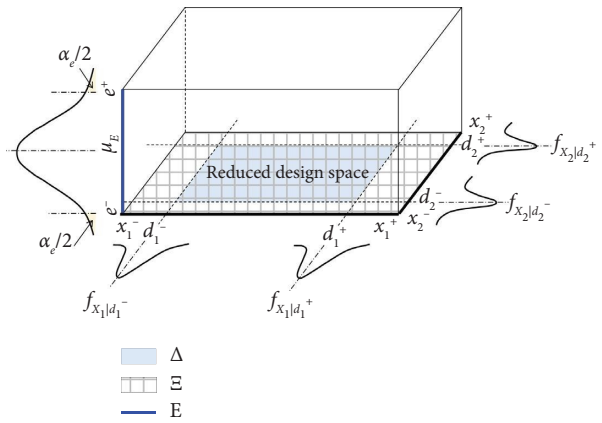

Figure 7: Illustration of an augmented space for a three-dimensional problem considering two design variables $X_1(d_1)$ and $X_2(d_2)$ and a random environmental variable E.

3.3. Learning Function and Stopping Criterion. To adaptively refine the Kriging model, many learning functions have been proposed to enrich the DoE of the metamodel, such as the U learning function and expected feasibility function (EFF). In this study, EFF is used as a learning criterion for the selection of additional training samples, which is defined as follows [55]:

$$\begin{aligned}\mathrm{EFF}(\mathbf{x}) = (\widehat{G}(\mathbf{x}) - a)\left[2\Phi\left(\frac{a-\widehat{G}(\mathbf{x})}{\sigma_{\widehat{G}}(\mathbf{x})}\right) - \Phi\left(\frac{(a-\varepsilon)-\widehat{G}(\mathbf{x})}{\sigma_{\widehat{G}}(\mathbf{x})}\right) - \Phi\left(\frac{(a+\varepsilon)-\widehat{G}(\mathbf{x})}{\sigma_{\widehat{G}}(\mathbf{x})}\right)\right] \\ - \sigma_{\widehat{G}}(x)\left[2\phi\left(\frac{a-\widehat{G}(\mathbf{x})}{\sigma_{\widehat{G}}(\mathbf{x})}\right) - \phi\left(\frac{(a-\varepsilon)-\widehat{G}(\mathbf{x})}{\sigma_{\widehat{G}}(\mathbf{x})}\right) - \phi\left(\frac{(a+\varepsilon)-\widehat{G}(\mathbf{x})}{\sigma_{\widehat{G}}(\mathbf{x})}\right)\right] \\ + \left[\Phi\left(\frac{(a+\varepsilon)-\widehat{G}(\mathbf{x})}{\sigma_{\widehat{G}}(\mathbf{x})}\right) - \Phi\left(\frac{(a-\varepsilon)-\widehat{G}(\mathbf{x})}{\sigma_{\widehat{G}}(\mathbf{x})}\right)\right],\end{aligned} \tag{28}$$

where Φ represents the standard normal CDF, ϕ is the standard normal probability density function (PDF), $\widehat{G}(\mathbf{x})$ is the predicted response at the location $\mathbf{x}$, and $\sigma_{\widehat{G}}(\mathbf{x})$ is the corresponding standard deviation. The value of EFF indicates how well the actual performance function value at the location $\mathbf{x}$ is expected to satisfy $\widehat{G}(\mathbf{x}) = a$ over the region $a \pm \varepsilon$. A large EFF value implies a high level of uncertainty in the predicted function value. Hence, $\mathbf{x}$ corresponding to the maximum EFF is selected as the point to be added to the training set. The next candidate sample is then selected by

$$\mathbf{x}* = \arg\max_{x \in S_{\mathrm{ED}}} \mathrm{EFF}(\mathbf{x}), \tag{29}$$

where S_{ED} denotes the candidate samples in the augmented space.

Furthermore, a convergence criterion needs to be adopted to terminate the addition of samples to the DoE when the trained metamodel is accurate enough for further use in reliability assessment and optimization. Here, the convergence criterion is defined as the stability of the failure probability estimate:

$$\frac{\left|\widehat{P}_f^{(j)} - \widehat{P}_f^{(j-1)}\right|}{\widehat{P}_f^{(j)}} \leq \varepsilon, \tag{30}$$

where $\widehat{P}_f^{(j)}$ represents the estimated failure probability at the j-th iteration and ε is the tolerance (or relative error in the probability estimate) and set as 0.001.

3.4. Optimization Method. To simultaneously consider two competing objectives, i.e., minimizing the interstory drift and average control force, NSGA-II is used to search for the optimal solution to construct reliable fuzzy logic controllers. In this multiobjective optimization algorithm, the solutions are first sorted into each front according to a nondomination rank, and then, the solutions of each front can be optimized for population diversity by representing each group of crowded points with a single point. For more details about NSGA-II, please refer to [56]. The main procedures of the NSGA-II-based optimization implemented in this study are illustrated in Figure 8.

3.5. Implementation Scheme. A double-loop strategy combined with the Kriging model and NSGA-II is used to construct optimum and robust fuzzy logic controllers for mitigating the seismic response of the MR damper-based structural system. For clarity, the implementation aspects are illustrated in Figure 9, and the basic steps are summarized as follows:

(1) Determine the design variables to form the original design space

(2) Narrow down the original design space by regulating the range of design variables and predesigning fuzzy rules based on control expertise

(3) Determine the distribution characteristics of both the design and environmental variables and then build the augmented space by extending the space of reduced design variables and environmental variables with the space of random variables

(4) Use the Latin hypercube sampling (LHS) method to generate the initial DoE $\mathcal{X} = \{\mathbf{x}^{(1)}, \ldots, \mathbf{x}^{(N_0)}; N_0 = 2(N_{\mathrm{d}} + N_{\mathrm{e}}) + 1\}$ and then evaluate the corresponding LSF responses $\mathcal{Y} = \{y^{(1)}, \ldots, y^{(N_0)}\} = \{g(\mathbf{x}^{(1)}), \ldots, g(\mathbf{x}^{(N_0)})\}$ by the computational model

(5) Train the Kriging model based on the current DoE $\{\mathcal{X}, \mathcal{Y}\}$

(6) Estimate the failure probability using Monte Carlo simulation with the current surrogate model $M^{(K)}$

(7) Choose the best next sample $\mathbf{x}^*$ to be added to the current DoE $\{\mathcal{X}, \mathcal{Y}\}$ based on the learning function EFF

(8) Check whether the stopping criterion is satisfied or the maximum number of added DoE, i.e., $N_{\mathrm{s,max}} = 600$, is reached. If it is, skip to Step (10), otherwise, continue with Step (9)

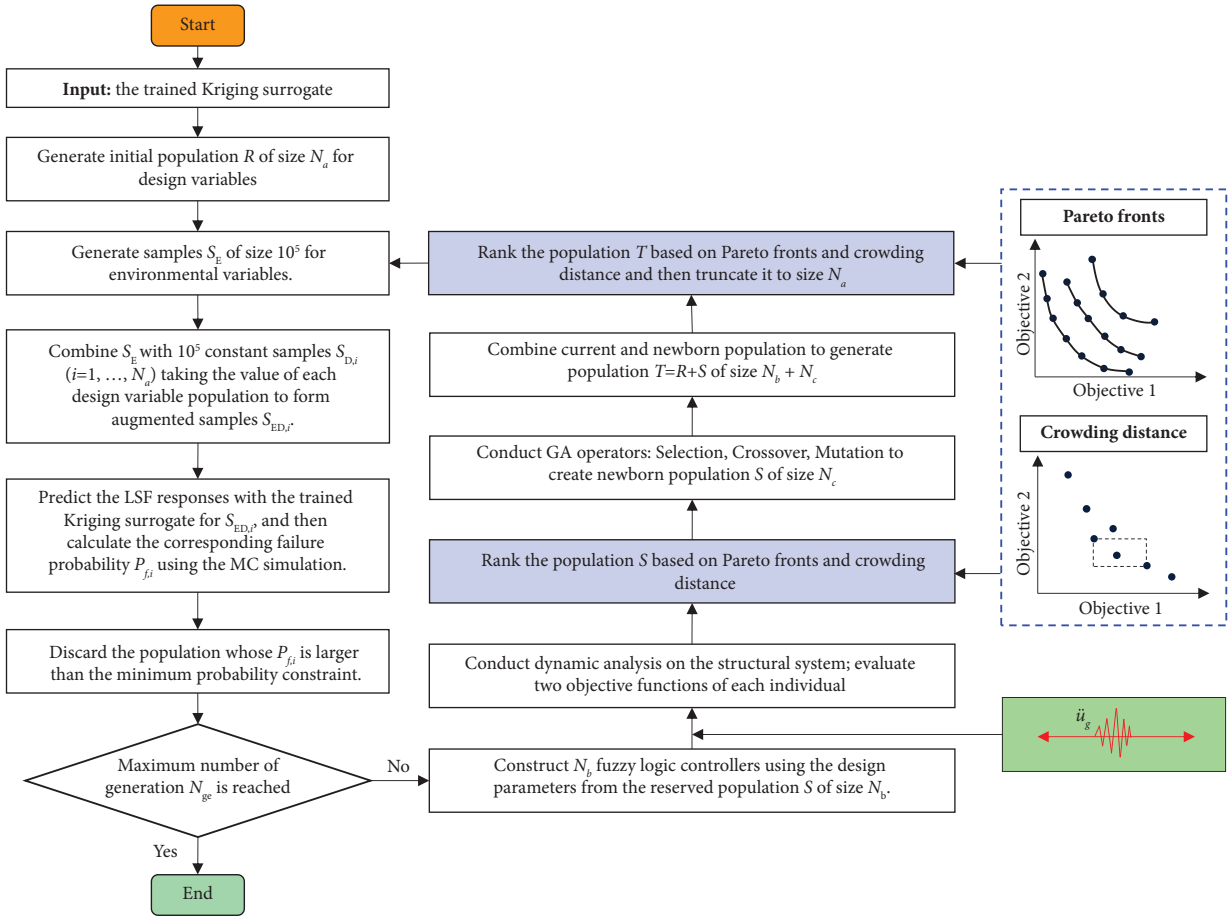

Figure 8: Flowchart of NSGA-II-based optimization.

(9) Add $\mathbf{x}^*$ and the corresponding LSF response to the DoE of the metamodel and return to Step (5)

(10) Obtain the final Kriging model with the predetermined accuracy

(11) Conduct the multiobjective RBDO for the MR damper-based structural system using the NSGA-II combined with the constructed Kriging model, see Figure 8

(12) Stop the optimization once the maximum number of iterations is reached.

4. Numerical Examples

In this section, multiobjective RBDO is employed to optimize fuzzy logic controllers for both linear and nonlinear structures.

4.1. 3-Story Linear Structure

4.1.1. Structural Model. The first numerical example is a three-story linear structure, in which a total of $N_e = 5$ independent random environmental variables are considered, including interstory stiffness (k_1, k_2, and k_3) and external excitations (θ_1 and θ_2). These random variables are all assumed to be lognormally distributed. The statistical information of these random variables and the mass of each structural floor are shown in Table 3. The height of each floor is taken as 3.0 m. Rayleigh damping is assumed for calculating the damping matrix $\mathbf{C}$ ($\mathbf{C} = a\ \mathbf{M} + b\ \mathbf{K}$), and the damping ratio is assumed as 5%. Based on the first two natural vibration periods of the structure, related damping coefficients are calculated: $a = 1.2574$ s and $b = 0.0016$ s. The maximum damping capacity of the MR damper is set as $F_{\max} = 1000$ kN under the maximum input current of 2 A by scaling the parameters involved in the forward dynamic model. The amplitude coefficient of input earthquake excitations is set as $\zeta = 0.2$ g, corresponding to a frequently occurred earthquake. In the Chinese seismic design code [57], it is specified that to keep the reinforced concrete frame structure remain in an elastic state, the maximum interstory drift of the structure should not exceed 1/550 of the floor height, i.e., $1/550 \times 3000 = 5.45$ mm, under a frequently occurred earthquake. This study applied this specification to define the threshold of maximum interstory drift for the linear structure. The failure probability of the uncontrolled structure is 0.47.

4.1.2. Comparison between Multiobjective RBDO and DDO. According to the multiobjective RBDO method presented in Section 3, the Kriging model is built in the 42-dimensional

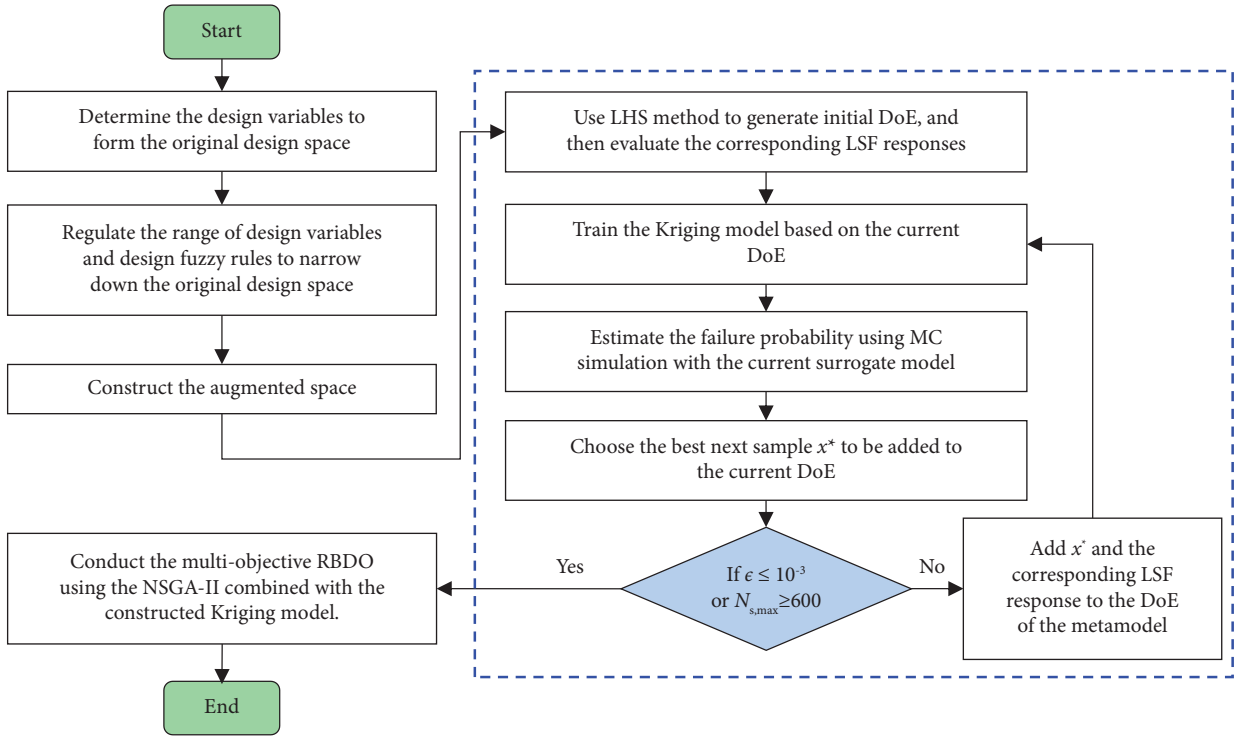

Figure 9: Flowchart of the proposed multiobjective RBDO method.

Table 3: Parameters of structural properties and input excitations.

Variables	Notification	Distribution	Mean	C.O.V.
Floor mass	M_i	—	3.8, 3.2, 2.3 ($\times 10^5$ kg)	—
Interstory stiffness	K_i	Lognormal	4.56, 4.16, 3.55 ($\times 10^8$ N/m)	0.1
Stochastic coefficient of N-S	θ_1	Lognormal	0.5	0.2
Stochastic coefficient of E-W	θ_2	Lognormal	0.5	0.2

($N_{\text{au}} = N_d + N_e = 37 + 5$) augmented space. First, LHS is employed to generate the initial DoE of size $N_0 = N_{\text{au}} \times 2 + 1 = 85$. Then, the learning function EFF (equation (28)) is employed to place as many training samples as possible in the neighborhood of the limit state, so as to refine adaptively the Kriging model, and 111 new training points are finally needed when the corresponding stopping condition in equation (30) is satisfied. As shown in Figure 10, there is still a misclassification of several samples with respect to the safe and failure domain, whereas the number of samples that are regarded as failure points but are actually in the safe domain (red dots) and the number of samples that are classified as safe points but are actually in the failure domain (blue dots) are approximately equal. As a result, the resultant failure probability $\widehat{P}_f$ is very close to its true counterpart.

With the trained Kriging model, the NSGA-II-based multiobjective optimization with an initial population size of $N_a = 100$ is conducted to search for optimal design solutions. The optimization results from different optimization generations in the form of Pareto fronts are compared in Figure 11(a). It is observed that, with the increasing number of optimization generations, the Pareto front is moving closer to the origin of coordinates, indicating the improvement of the quality of the elite individuals. Here, the Pareto front is assumed to be converged at 100 generations as the Pareto fronts of the last two optimization generations, i.e., $N_{\text{ge}} = 80$ and $N_{\text{ge}} = 100$, are highly overlapped.

As a comparison to multiobjective RBDO, the multiobjective DDO is also employed here for solving the same optimization problem. The only difference between the two approaches is that there is no probability constraint in the latter approach. The multiobjective DDO-derived solutions are shown in Figure 11(b). It is seen that the Pareto front also converges as fast when there is no probability constraint. It is mainly because the design space has been narrowed down into a relatively small and reasonable range, which can save much computational cost. Besides, it is worth noting that the Pareto fronts derived from the RBDO are a bit closer to the Y-axis than those derived from DDO, indicating the RBDO-derived solutions can achieve a better control performance.

Furthermore, the failure probability of the linear structural system under the design solutions obtained from multiobjective RBDO and DDO is, respectively, calculated and compared in Figure 12. It is observed that some DDO-derived solutions show relatively high failure probability, while the solutions obtained from RBDO all show very low

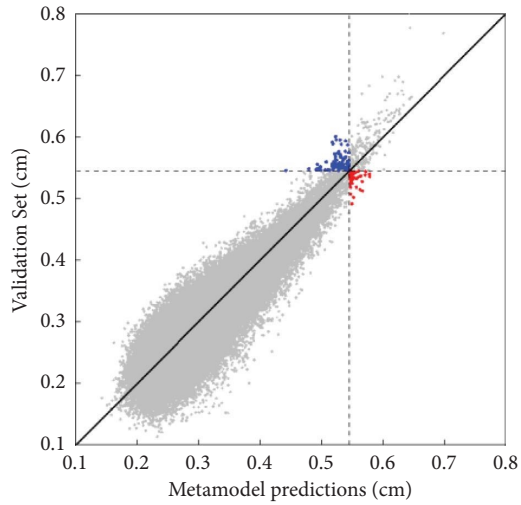

FIGURE 10: Validation of the trained Kriging model.

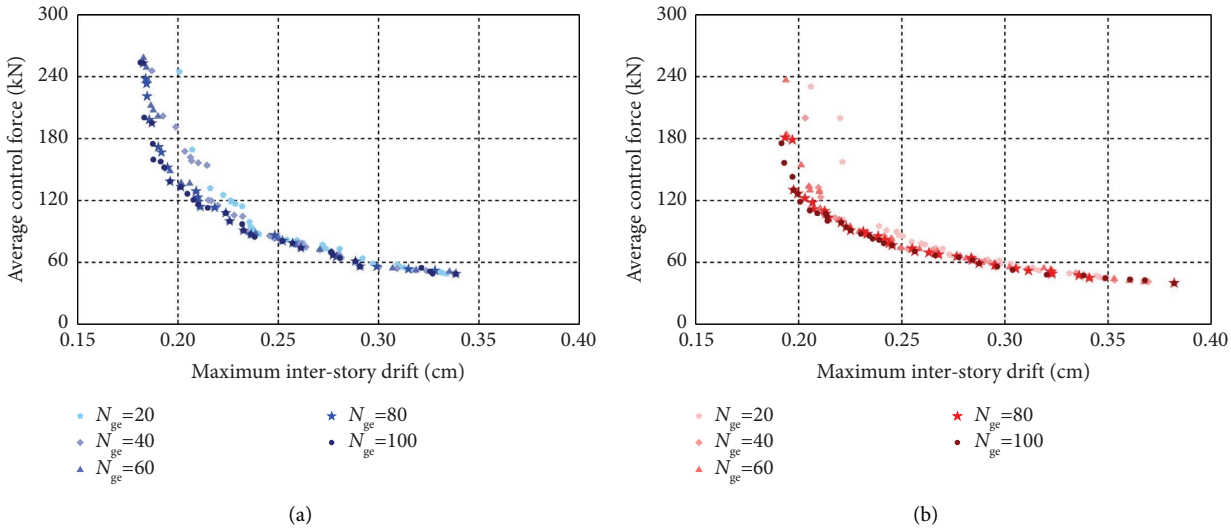

FIGURE 11: Comparison between the Pareto fronts obtained from multiobjective RBDO (a) and DDO (b).

failure probability due to the consideration of probability constraint. Therefore, it is necessary to take the uncertainties into account for obtaining more reliable fuzzy logic controllers.

To further verify the robustness of the optimized fuzzy logic controllers, the design solutions from $N_{ge} = 100$ optimization generations of DDO and RBDO are used. Corresponding maximum interstory drift and floor acceleration responses of the structural system with 25% stiffness degradation are compared in Figure 13(a). It is observed that the maximum interstory drift responses of the structural system utilizing the RBDO- and DDO-derived fuzzy logic controllers are all much lower than the uncontrolled structural responses, but the maximum floor acceleration responses of several controlled cases are larger than those of the uncontrolled case. It is mainly because there is a trade-off between interstory drift and floor acceleration responses, and minimizing the interstory drift may have an adverse effect on floor acceleration. Therefore, the solutions which can minimize the interstory drift mostly show the worst performance in reducing floor acceleration. For both interstory drift and floor acceleration responses, the RBDO-derived fuzzy logic controllers show better control performance than the DDO-derived ones, indicating superior robustness. In the meantime, the robustness of the optimized fuzzy logic controllers to the uncertainty associated with external excitations is also verified, as shown in Figure 13(b). Here, three ground motion records collected from different earthquake events, i.e., Imperial Valley (1979), Hachinohe (1968), and Kobe (1995), are scaled to have a peak acceleration of 0.2 g and then used as external excitation. It is observed that the fuzzy logic controllers obtained from RBDO and DDO both show good control performance under different earthquake excitations, but apparently, the RBDO-derived controllers show more robustness than the DDO-derived ones.

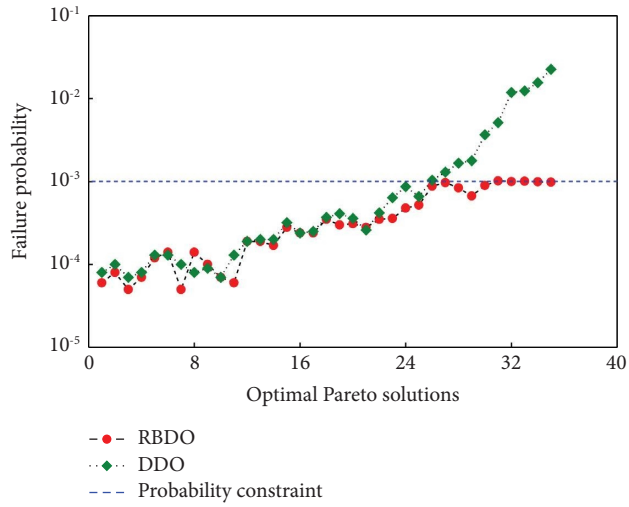

Figure 12: Failure probability of the linear structural system using the DDO- and RBDO-derived optimal solutions.

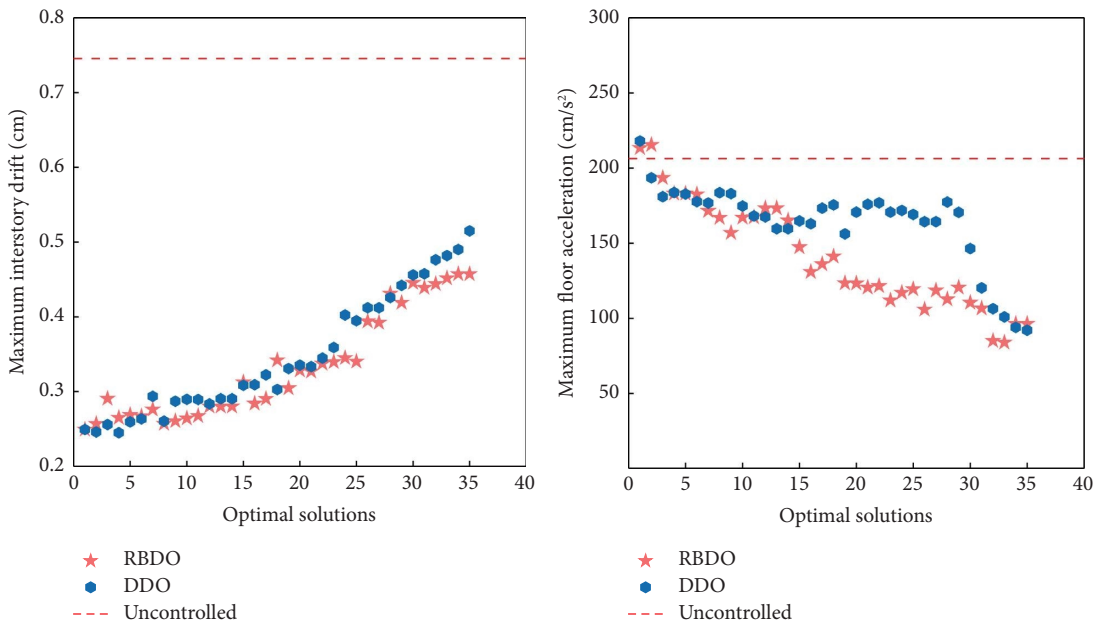

(a)

Figure 13: Continued.

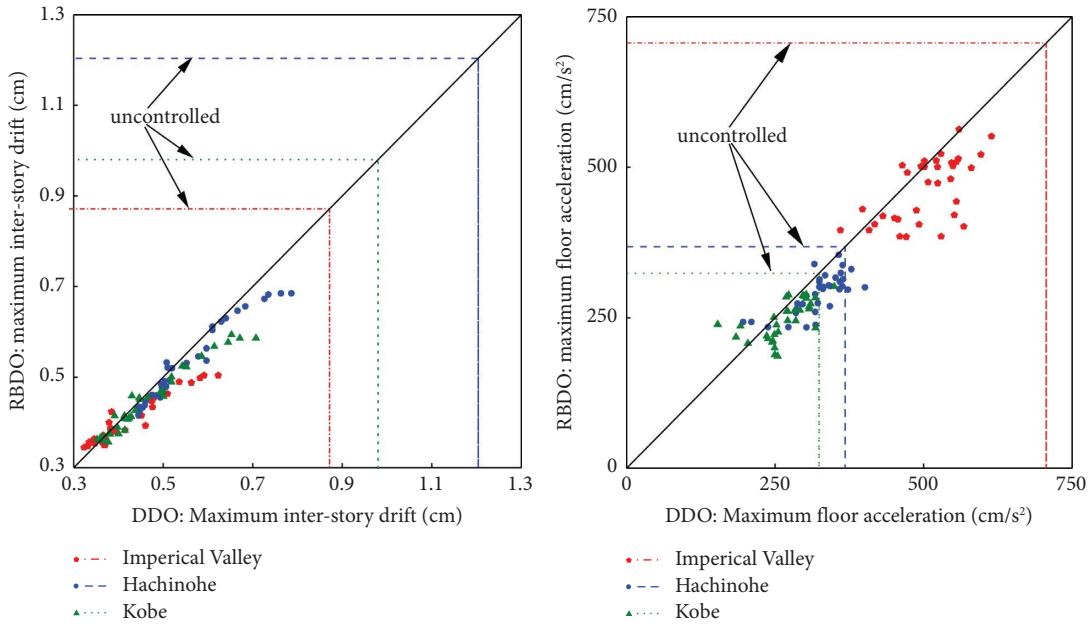

(b)

Figure 13: Comparison between the multiobjective RBDO- and DDO-derived optimal solutions: (a) stiffness degradation (25%); (b) different earthquake excitations.

4.1.3. Parameter Analysis. To probe the characteristics of the RBDO-derived optimal solutions, the solutions from the final optimization generation ($N_{ge} = 100$) are selected for analysis here. For clarity, these solutions are first normalized by the bounds of the design space and then mapped into a 37-dimensional polygon. In the polygon-based design space, the upper and lower bounds of a design variable are, respectively, represented by the vertex and the center of the polygon.

Figure 14(a) shows the RBDO-derived solutions, which are represented by blue-filled triangles and constrained in two black dash curves, respectively, representing the upper and lower bounds of the solutions. It is observed that these solutions mostly gather in the central zone of the design space, indicating the rationality of the reduced design space. As a comparison, the DDO-derived optimal solutions ($N_{ge} = 100$) are illustrated in Figure 14(b), in which the solutions of low ($P_f \leq 10^{-3}$) and high ($P_f > 10^{-3}$) failure probability are, respectively, represented by gray-filled circles and red spheres. It is seen that the DDO-derived solutions, especially for those of high failure probability, are more scattered and closer to the bounds of the design space than the RBDO-derived solutions. Figures 14(c) and 14(d) show that the RBDO-derived solutions can be largely enclosed by the domain defined by the lower and upper bounds of the DDO-derived solutions, especially for the solutions from a relatively lower optimization generation, i.e., $N_{ge} = 20$, as the optimal solutions are more concentrated with the increasing optimization generations. In this respect, the multiobjective DDO method can be used to locate a relative safety domain for simplifying some complex, nonlinear RBDO problems, because RBDO only searches for optimal solutions in the domain where the probability constraint is satisfied.

4.2. 10-Story Nonlinear Structure

4.2.1. Structural Model. Here, a ten-story nonlinear structure is investigated, and a total of $N_e = 12$ independent random environmental variables concerning initial interstory stiffness ($k_1, \ldots, k_{10}$) and external excitations (θ_1 and θ_2) are considered, which are all assumed to be lognormally distributed. Detailed information regarding structural properties and earthquake excitations is listed in Table 4. The height of each floor is taken as 3.0 m. Rayleigh damping is utilized here, with the damping ratio being 0.05. Corresponding coefficients are $a = 0.3242$ s and $b = 0.0063$ s. The maximum damping capacity of the MR damper is also set as 1000 kN here. The amplitude coefficient of input earthquake excitations is set as $\zeta = 0.4$ g, corresponding to a rarely occurred earthquake. According to the Chinese seismic design code [57], to keep the reinforced concrete frame structure remain in an elastic-plastic state, the maximum interstory drift of the structure should not exceed 1/50 of the floor height, i.e., $1/50 \times 300 = 6$ cm, under a rarely occurred earthquake. The failure probability of this uncontrolled nonlinear structure is 0.03. The nonlinear interstory hysteretic behavior is considered and represented by the Bouc–Wen model [58, 59], as shown in Figure 15. The parameters of the Bouc–Wen model are deterministic, as a reference to the literature [59].

4.2.2. Metamodel Training. For the nonlinear structure investigated here, the Kriging model is trained in a 49-dimensional ($N_{au} = N_d + N_e = 37 + 12$) augmented space with an initial DoE of size $N_0 = (N_d + N_e) \times 2 + 1 = 99$. However, before training the Kriging model for the

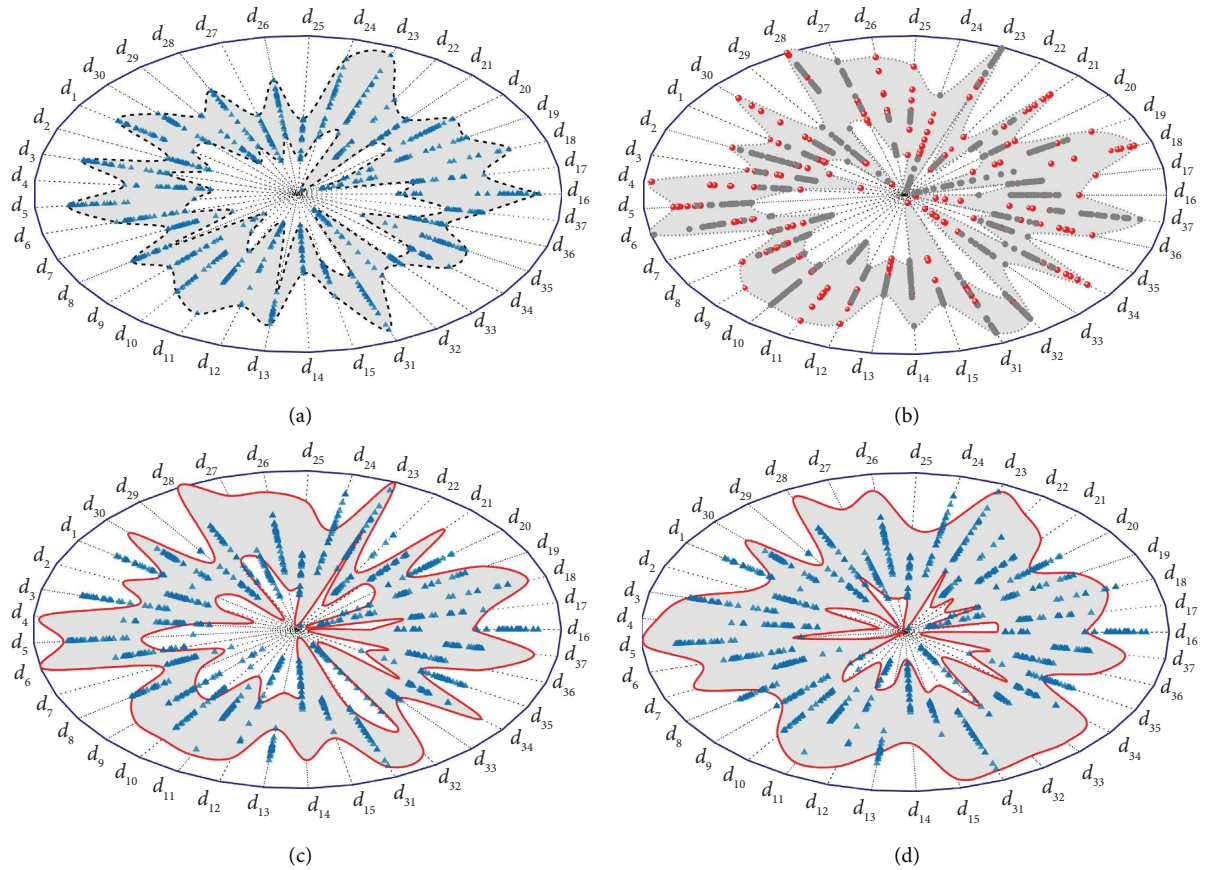

FIGURE 14: Relative position of the optimum solutions derived by multiobjective RBDO and DDO. (a) RBDO-derived solutions ($N_{ge} = 100$). (b) DDO-derived solutions ($N_{ge} = 100$). (c) RBDO-derived solutions in the range defined by the DDO-derived solutions of $N_{ge} = 100$. (d) RBDO-derived solutions in the range defined by the DDO-derived solutions of $N_{ge} = 20$.

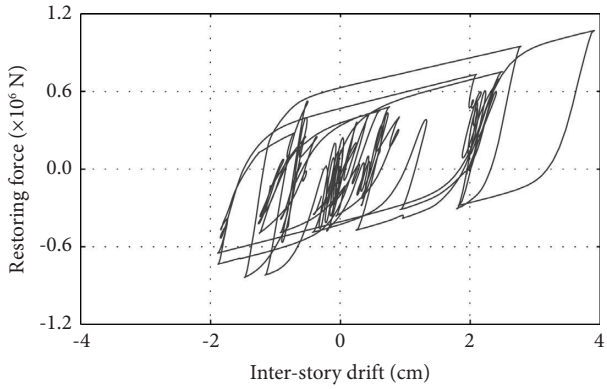

FIGURE 15: Curve of the Bouc–Wen model.

TABLE 4: Statistical properties of random variables.

Random variables	Notification	Distribution	Mean	C.O.V.
Floor mass	M_i	—	4.50, 4.14, 3.78, 3.15, 2.97, 2.88, 2.88, 2.79, 2.52, 2.25 ($\times 10^5$ kg)	—
Interstory stiffness	K_i	Lognormal	3.36, 3.12, 2.76, 2.52, 2.40, 2.10, 1.68, 1.50, 1.20, 1.20 ($\times 10^8$ N/m)	0.1
Stochastic coefficient of N-S	θ_1	Lognormal	0.5	0.1
Stochastic coefficient of E-W	θ_2	Lognormal	0.5	0.1

nonlinear structure, it is worth noting that metamodel training for a nonlinear structure is usually much more difficult than for a linear structure due to the nonlinearity and associated complexity of structural dynamics. Besides, compared with the investigated linear structure, the dimension of the augmented space of the nonlinear structure is increased and the uncontrolled structural failure probability is decreased, which further increases the difficulty of building an accurate Kriging model for the nonlinear structure. It is worth noting that RBDO only searches for optimal solutions in the safety domain, where the probability constraint is always satisfied, i.e., $P_f \leq P_{f0}$. Therefore, the constructed surrogate model should have sufficient prediction accuracy for evaluating samples within the safety domain, while the prediction accuracy for samples out of the safety domain can be relaxed, which can reduce the training samples required by metamodel training.

For clarity, a simple illustration of locating a safety domain in a two-dimensional augmented space is shown in Figure 16, in which the LSF line-enclosed area is filled with failure points (red) and the other area is full of safe points. It is seen that, when the design variable takes the value of x_2, x_4, x_5, or x_7, the failure probability P_f equals the target failure probability P_{f0}. Since LSF can be represented by the simple analytical expression, the safety domain, i.e., $[x^-, x_2]$, $[x_4, x_5]$, and $[x_7, x^+]$, can be easily identified. However, it is not an easy task to locate the safety domain for a complicated, realistic engineering problem that cannot be described with explicit analytical expressions. According to the analysis presented in Section 4.1.3, the RBDO-derived optimal solutions can be largely covered within the range defined by the lower and upper bounds of the DDO-derived optimal solutions. Therefore, to more effectively solve the optimization problem of fuzzy logic controllers for the nonlinear structure, multiobjective DDO can be preconducted to locate a rough safety domain. The main implementation procedures are listed as follows: first, multiobjective DDO is conducted for 20 generations, and the lower and upper bounds of the obtained optimal solutions are defined as the safety domain; then, the safety domain-based design space is combined with the random environmental space to construct an augmented space, where the surrogate model is trained, and finally, multiobjective RBDO is conducted for searching optimal solutions based on the trained metamodel.

The process of the Kriging model trained in the safety domain-based augmented space is shown in Figure 17(a). It is observed that the stopping condition is finally satisfied with less than 160 new training points. Figure 17(b) shows that the metamodel predictions agree well with the computational model evaluations in the neighborhood of the limit state, which effectively ensures the high accuracy of the failure probability estimate. The metamodel is also trained in the original augmented space for comparison. The corresponding training process is shown in Figure 18(a), in which 600 additional new training points have been sequentially added, but the stopping condition has not been reached. The trained model is then used to predict the structural interstory drift responses and compared with the computational model evaluations, as shown in Figure 18(b). It is seen that there is a large discrepancy between the results derived by the metamodel and computational model, indicating the inaccuracy of the trained surrogate model. Therefore, prelocating a safety domain can effectively improve the efficiency of training a desired metamodel for complex, nonlinear structures.

4.2.3. Optimization Results and Analysis. With the well-trained Kriging model, multiobjective RBDO is then carried out for searching for optimal FLC designs for the nonlinear structure. The optimal solutions derived from different optimization generations are illustrated in Figure 19(a). It is seen that the Pareto front is moving closer to the origin with the increasing generations and finally converging at 200 generations. The solutions from the final optimization generation are then mapped into the original design space represented by a 37-dimensional polygon, see Figure 19(b). These optimal solutions are represented by gray-filled circles enclosed in the DDO-provided safety domain denoted by the shadow area surrounded by two black dash curves. As can be seen, the solutions of each design variable are quite close to each other in the design space due to the probability constraint.

For further analysis, three solutions corresponding to different control force levels, i.e., $F_{\text{ave}} = 60$, 70, and 80 kN, are selected from the final optimization generation and highlighted in colorful spheres, see Figure 19(b). The membership functions corresponding to the selected solutions are depicted in Figure 20. It is observed that the difference between the input or output membership functions of the three selected solutions is minor in terms of shape, and the obvious distinction only exists in the range of the output membership function, which has determined the control force level.

Based on the selected solutions mentioned above, three fuzzy logic controllers are obtained, denoted as Controller 1 ($F_{\text{ave}} = 60$ kN), Controller 2 ($F_{\text{ave}} = 70$ kN), and Controller 3 ($F_{\text{ave}} = 80$ kN), and then used to control the seismic response of the nonlinear structure. The peak interstory drift and floor acceleration of the controlled and uncontrolled nonlinear structures are compared in Figure 21(a). It is observed that both the interstory drift and floor acceleration are reduced when fuzzy logic controllers are applied, and the interstory drifts are decreased with the increasing average control force. One may notice that the maximum interstory drift responses of the controlled and uncontrolled structures both appear on the first floor, which can be regarded as the weak floor. Therefore, the original damper distribution, i.e., one damper for each floor, is rearranged here by transferring the top floor damper to the first floor and keeping the other floors unchanged. Then, the peak interstory drift responses of the rearranged structural system under the three selected fuzzy logic controllers are, respectively, recalculated, as shown in Figure 21(b). It is seen that the selected fuzzy logic controllers still work well when the damper distribution is slightly rearranged and even better control performance is achieved, especially for the weak floor. Therefore, the seismic

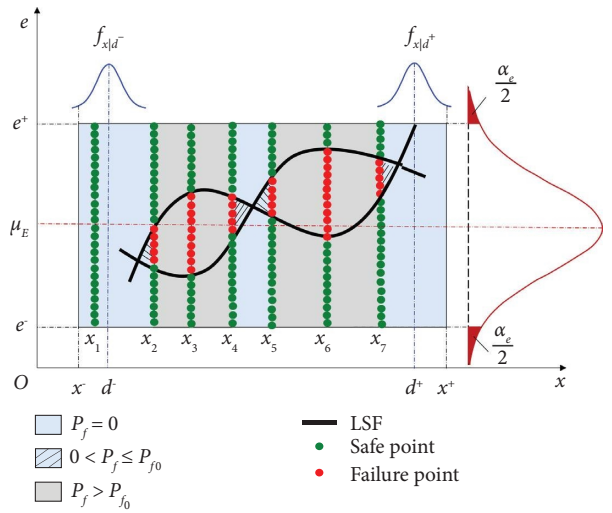

Figure 16: Illustration of safe and failure domains in an augmented space.

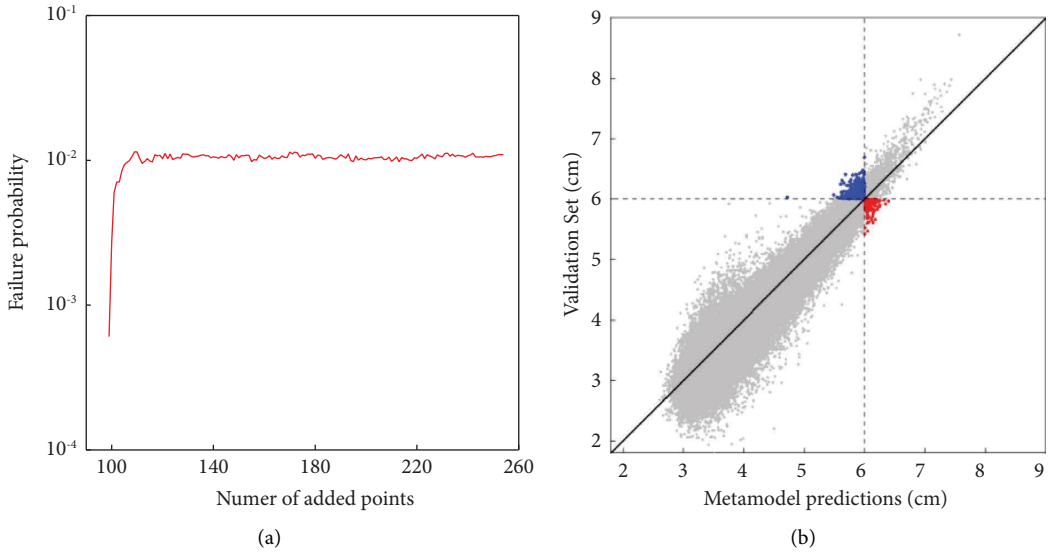

Figure 17: Metamodel training in the safety domain-based augmented space: (a) training process of the metamodel; (b) validation of the metamodel.

performance of a controlled structure with a specified FLC configuration may be further improved by optimizing the damper distribution. In this respect, an NSGA-II-based multiobjective deterministic optimization is then conducted on the nonlinear structure under the control of the three selected controllers for finding an optimal damper distribution. The corresponding optimization problem is formulated as follows:

$$\begin{aligned} &\text{find } \mathbf{p} = [p_1, p_2, \ldots, p_{10}], \\ &\min \mathbf{c} = [S_{\max}(\mathbf{p}), F_{\text{ave}}(\mathbf{p})], \\ &\text{s.t.} \begin{cases} 0 \le p_i \le 3, & (i = 1, \ldots, 10), \\ N_{\text{MR}} = \text{sum}(p_i) \le 10, & (i = 1, \ldots, 10), \end{cases} \end{aligned} \tag{31}$$

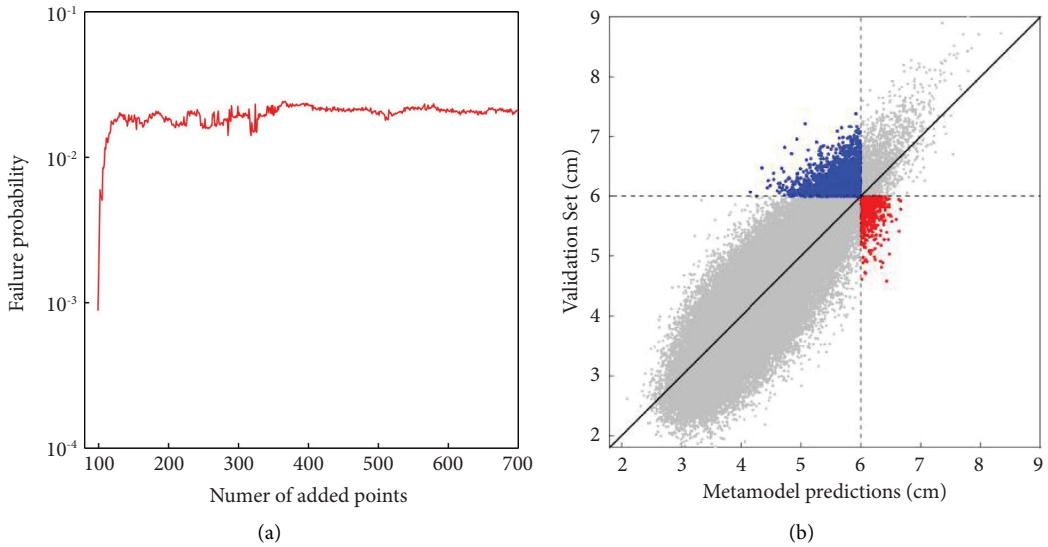

FIGURE 18: Metamodel training in the original augmented space: (a) training process of the metamodel; (b) validation of the metamodel.

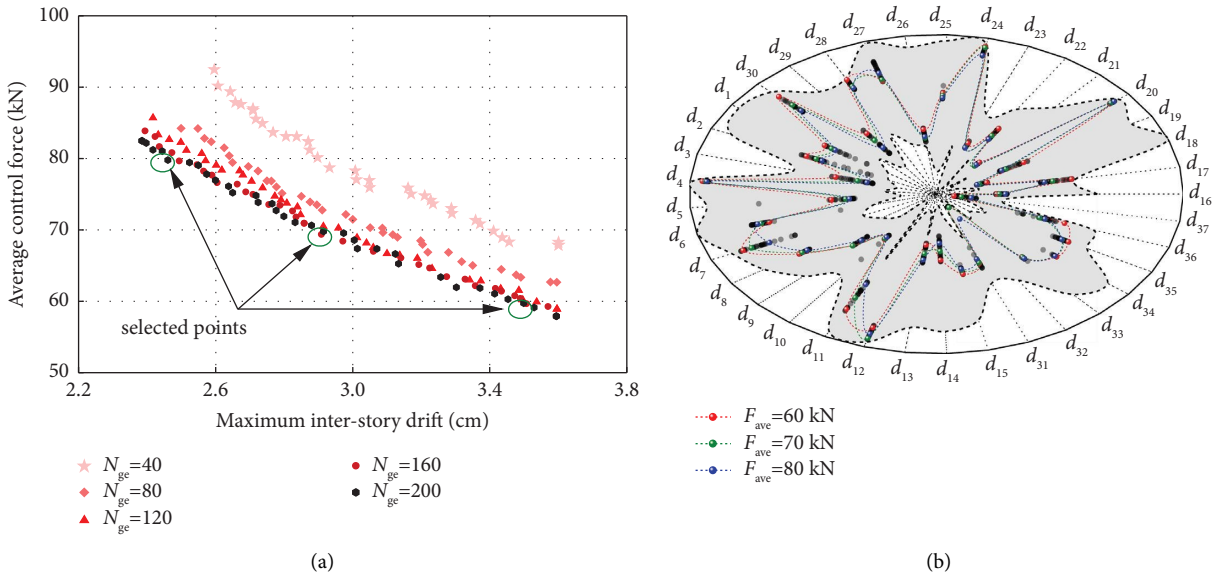

FIGURE 19: Optimal solutions to the fuzzy logic controllers of the nonlinear structural system: (a) Pareto fronts of different optimization generations; (b) optimal design solutions.

where p_i denotes the number of MR dampers on the i-th floor and N_{MR} represents the total number of MR dampers. Here, in view of damper size restriction and the economical aspect, two soft constraints are considered for restricting the quantities of MR dampers on each floor and total floors.

The optimization results in terms of the Pareto front are shown in Figure 22. As a comparison, the optimization results corresponding to Controllers 1, 2, and 3 for the evenly distributed MR damper-based structure are also depicted in Figure 22, which are respectively represented by the hollow circle, square, and triangular. As can be seen, with consideration of optimizing damper distribution, the maximum interstory drift responses can be further decreased, and correspondingly, a higher average control force level is required. It is also observed that the Pareto front of the controller corresponding to a lower control force level is closer to the origin of coordinates, indicating a better structural system in terms of mitigating structural response and saving control cost. Among all the solutions shown in Figure 22, most solutions have applied 10 MR dampers, and only 5 solutions have used fewer than 10 MR dampers, which are labeled with ①, ②, ③, ④, and ⑤, respectively, corresponding to 8, 7, 9, 9, and 9 MR dampers. The damper distributions corresponding to these 5 solutions are shown in Figures 23(a)–23(e). It is observed that MR dampers mostly concentrate on the bottom and upper floors. The reason behind this phenomenon is that the seismic forces exerted on the bottom floors are relatively larger than those

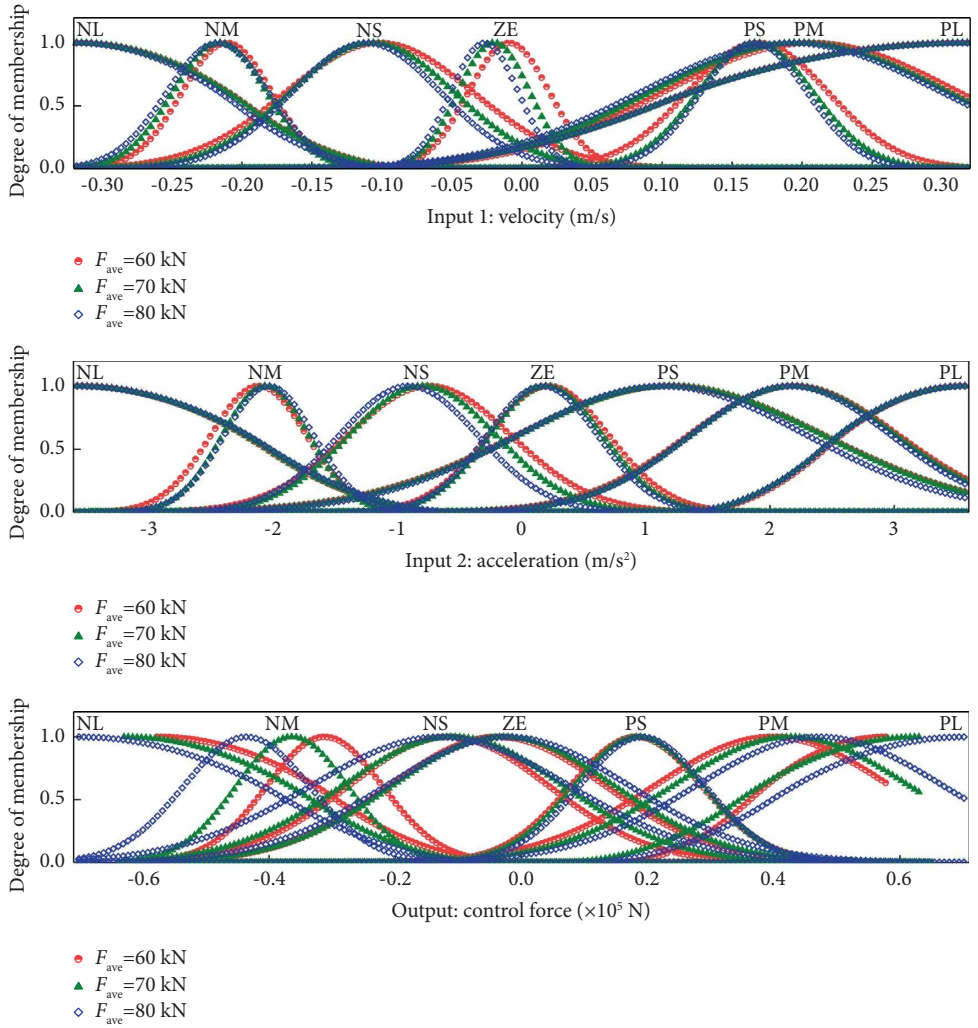

Figure 20: Membership functions of three selected solutions.

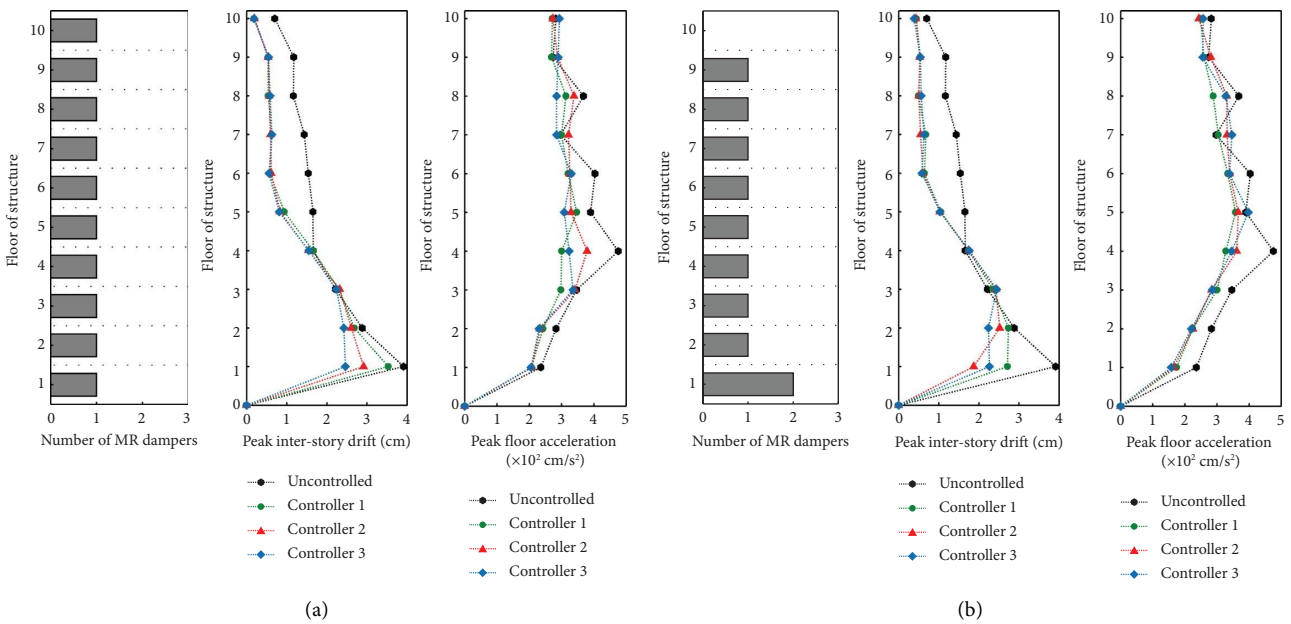

Figure 21: Peak interstory drift and floor acceleration versus structural floor of different damper distributions: (a) original damper distribution; (b) rearranged damper distribution.

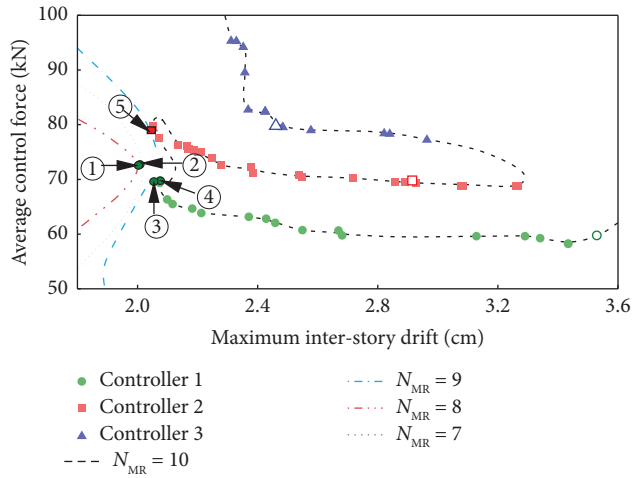

FIGURE 22: Optimization results regarding MR damper distribution.

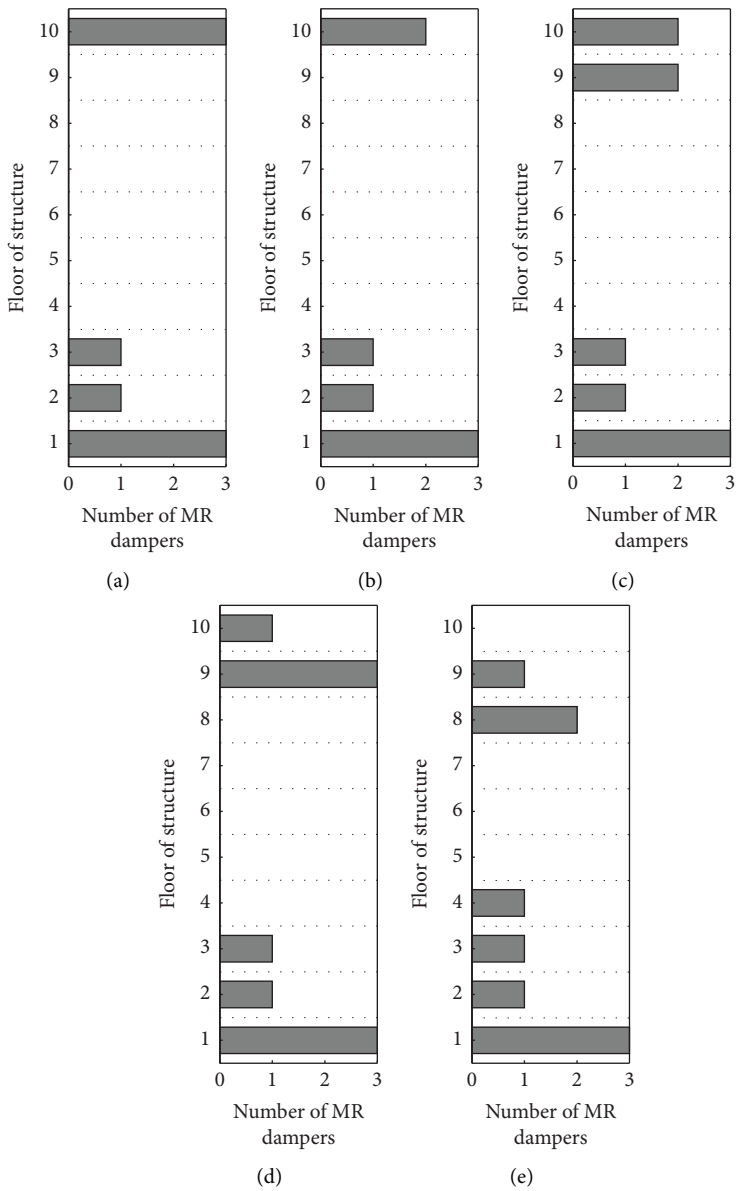

FIGURE 23: Continued.

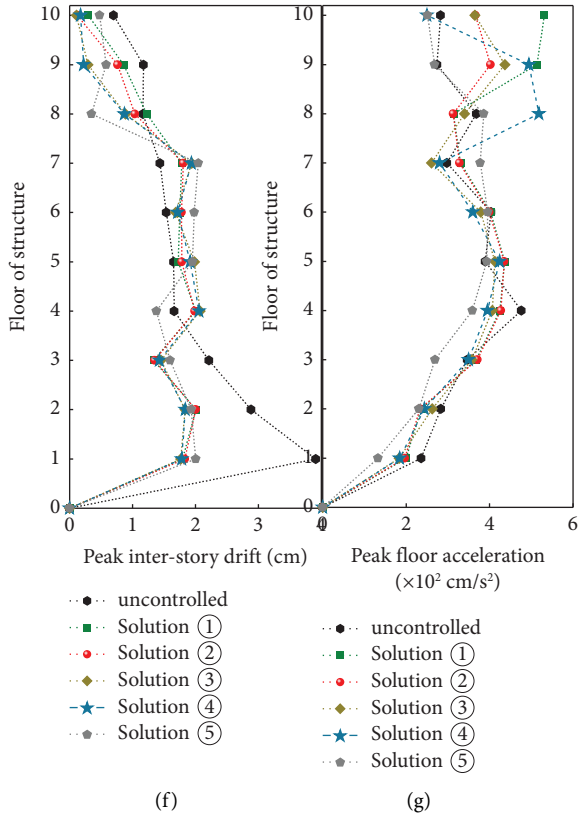

Figure 23: Damper distribution and corresponding controlled structural response from different solutions. (a) Damper distribution of solution ①. (b) Damper distribution of solution ②. (c) Damper distribution of solution ③. (d) Damper distribution of solution ④. (e) Damper distribution of solution ⑤. (f) Peak interstory drift versus structural floor. (g) Peak floor acceleration versus structural floor.

exerted on other floors, and the structure stiffness of the upper floors is relatively smaller than that of other floors. Furthermore, compared with the peak interstory drift responses of the controlled structure applying evenly distributed dampers (Figure 21(a)), the peak interstory drift responses of the controlled structure applying the optimized damper distributions are relatively smaller and more uniform (Figure 23(f)). However, the peak floor acceleration responses are not as optimistic as the maximum interstory drift responses. For solutions ①~④, the acceleration responses are increased when the damper positions are optimized, especially for the upper floors. Only solution ⑤ still shows good control performance on both interstory drift and floor acceleration responses. Therefore, solution ⑤ is selected as the most optimal damper distribution here, because it not only reduces the number of MR dampers but also greatly alleviates the interstory drift and floor acceleration responses without increasing the control force level too much. It may be concluded that an appropriate damper distribution is not only beneficial for enhancing the structural performance but also for saving the control cost.

5. Conclusion

This paper contributes to devising optimum and robust fuzzy logic controllers for MR damper-based structural systems whose parameters are modeled in a probabilistic framework. To reduce the computational cost, the design space is first narrowed down by adjusting the range of design parameters and predefining the fuzzy rules according to the control expertise. An augmented space is then constructed by combining the narrowed design space and random environmental space, based on which a global Kriging model is adaptively trained for replacing the time-consuming computational model evaluations involved in reliability assessment. Finally, the trained metamodel combined with NSGA-II is integrated into the framework of RBDO for solving the FLC optimization problem of both linear and nonlinear structural systems. The main conclusions are summarized as follows:

(1) Both the multiobjective DDO and RBDO are capable of generating well-distributed optimal Pareto solutions to the FLC design, but the fuzzy logic controllers optimized by the probabilistic optimization framework present better reliability and robustness than those optimized by the conventional deterministic optimization framework.

(2) Multiobjective DDO can be used to locate a coarse safety domain for facilitating the implementation of multiobjective RBDO, as the RBDO-derived solutions can be largely enclosed by the domain defined by the lower and upper bounds of the DDO-derived solutions.

(3) For complex, nonlinear structures, using the multiobjective DDO to prelocate a rough safety domain can significantly reduce the number of samples for training the metamodel and further improve the efficiency of searching for optimal design solutions.

(4) The input or output membership functions of different optimal solutions are similar in terms of shape, and obvious distinction exists in the range of the output membership function, which has determined the control force level.

(5) The performance of a controlled structure with a specified FLC configuration can be further improved by considering the damper distribution optimization, especially for the structure with a relatively low-control-force-level controller.

It may be generally concluded that, for simple linear structural systems, multiobjective RBDO is an efficient and feasible approach for searching for optimal and reliable FLC designs. For complex, nonlinear structural systems, a safety domain needs to be predefined before conducting multiobjective RBDO. The safety domain provided by multiobjective DDO is a coarse estimate, and the number of DDO optimization generations used is based on experience. Therefore, further study on proposing a more reliable approach to locate the safety domain needs to be conducted in the future.

Data Availability

The data used to support the findings of this study are available from the corresponding author upon request.

Conflicts of Interest

The authors declare that they have no conflicts of interest.

Acknowledgments

The supports of the National Natural Science Foundation of China (Grant no. 51878505) and the Committee of Science and Technology of Shanghai China (Grant nos. 22160713000 and 21ZR1425500) are highly appreciated. The first author gratefully acknowledges the financial support from the China Scholarship Council (Grant no. 202106260175) for her study at the National University of Singapore.

References

[1] H. Akehashi and I. Takewaki, "Resilience evaluation of elastic-plastic high-rise buildings under resonant long-duration ground motion," *Japan Architectural Review*, vol. 5, no. 4, pp. 373–385, 2022.

[2] D. De Domenico, G. Ricciardi, and I. Takewaki, "Design strategies of viscous dampers for seismic protection of building structures: a review," *Soil Dynamics and Earthquake Engineering*, vol. 118, pp. 144–165, 2019.

[3] H. Akehashi and I. Takewaki, "Bounding of earthquake response via critical double impulse for efficient optimal design of viscous dampers for elastic-plastic moment frames," *Japan Architectural Review*, vol. 5, no. 2, pp. 131–149, 2022.

[4] I. Takewaki and H. Akehashi, "Comprehensive review of optimal and smart design of nonlinear building structures with and without passive dampers subjected to earthquake loading," *Frontiers in Built Environment*, vol. 7, Article ID 631114, 2021.

[5] H. J. Jung, K. M. Choi, B. F. Spencer, and I. W. Lee, "Application of some semi-active control algorithms to a smart base-isolated building employing MR dampers," *Structural Control and Health Monitoring*, vol. 13, no. 2-3, pp. 693–704, 2006.

[6] Y. B. Peng, R. Ghanem, and J. Li, "Generalized optimal control policy for stochastic optimal control of structures: generalized control policy for stochastic optimal control," *Structural Control and Health Monitoring*, vol. 20, no. 2, pp. 187–209, 2013.

[7] G. W. Housner, L. A. Bergman, T. K. Caughey et al., "Structural control: past, present, and future," *Journal of Engineering Mechanics*, vol. 123, no. 9, pp. 897–971, 1997.

[8] Y. B. Peng and Z. K. Zhang, "Optimal MR damper–based semiactive control scheme for strengthening seismic capacity and structural reliability," *Journal of Engineering Mechanics*, vol. 146, no. 6, p. 16, Article ID 04020045, 2020.

[9] F. Pozo, A. Rodriguez, L. Acho, Y. Vidal, and J. Rodellar, "Force-derivative feedback semi-active control of base-isolated buildings using large-scale MR fluid dampers," *Structural Control and Health Monitoring*, vol. 19, pp. 1839–1845, 2011.

[10] Z. Chen, X. Wang, J. Ko et al., "MR damping system for mitigating wind-rain induced vibration on Dongting Lake Cable-Stayed Bridge," *Wind and Structures*, vol. 7, no. 5, pp. 293–304, 2004.

[11] S. S. Sahasrabudhe and S. Nagarajaiah, "Semi-active control of sliding isolated bridges using MR dampers: an experimental and numerical study," *Earthquake Engineering and Structural Dynamics*, vol. 34, no. 8, pp. 965–983, 2005.

[12] T. Asai, C. M. Chang, B. M. Phillips, and B. F. Spencer, "Real-time hybrid simulation of a smart outrigger damping system for high-rise buildings," *Engineering Structures*, vol. 57, pp. 177–188, 2013.

[13] C. M. Chang, Z. Wang, B. F. Spencer, and Z. Chen, "Semi-active damped outriggers for seismic protection of high-rise buildings," *Smart Structures and Systems*, vol. 11, no. 5, pp. 435–451, 2013.

[14] S. J. Dyke, B. F. Spencer, M. K. Sain, and J. D. Carlson, "Modeling and control of magnetorheological dampers for seismic response reduction," *Smart Materials and Structures*, vol. 5, no. 5, pp. 565–575, 1996.

[15] S. J. Dyke, B. F. Spencer, M. K. Sain, and J. D. Carlson, "An experimental study of MR dampers for seismic protection," *Smart Materials and Structures*, vol. 7, no. 5, pp. 693–703, 1998.

[16] O. Yoshida and S. J. Dyke, "Seismic control of a nonlinear benchmark building using smart dampers," *Journal of Engineering Mechanics*, vol. 130, no. 4, pp. 386–392, 2004.

[17] K.-V. Yuen, Y. Shi, J. L. Beck, and H.-F. Lam, "Structural protection using MR dampers with clipped robust reliability-based control," *Structural and Multidisciplinary Optimization*, vol. 34, no. 5, pp. 431–443, 2007.

[18] D. A. Pohoryles and P. Duffour, "Adaptive control of structures under dynamic excitation using magneto-rheological dampers: an improved clipped-optimal control algorithm," *Journal of Vibration and Control*, vol. 21, no. 13, pp. 2569–2582, 2015.

[19] S. Dyke and B. Spencer, "A comparison of semi-active control strategies for the MR damper," in *Proceedings of the Intelligent*

Information Systems. IIS'97, pp. 580–584, IEEE, Grand Bahama Island, Bahamas, December 1997.

[20] L. M. Jansen and S. J. Dyke, "Semiactive control strategies for MR dampers: comparative study," *Journal of Engineering Mechanics*, vol. 126, no. 8, pp. 795–803, 2000.

[21] Z. D. Xu, Y. P. Shen, and Y. Q. Guo, "Semi-active control of structures incorporated with magnetorheological dampers using neural networks," *Smart Materials and Structures*, vol. 12, no. 1, pp. 80–87, 2003.

[22] S. M. A. Hashemi, H. Haji Kazemi, and A. Karamodin, "Localized genetically optimized wavelet neural network for semi-active control of buildings subjected to earthquake," *Structural Control and Health Monitoring*, vol. 23, no. 8, pp. 1074–1087, 2016.

[23] K. M. Choi, S. W. Cho, H. J. Jung, and I. W. Lee, "Semi-active fuzzy control for seismic response reduction using magnetorheological dampers," *Earthquake Engineering and Structural Dynamics*, vol. 33, no. 6, pp. 723–736, 2004.

[24] S. Y. Ok, D. S. Kim, K. S. Park, and H. M. Koh, "Semi-active fuzzy control of cable-stayed bridges using magneto-rheological dampers," *Engineering Structures*, vol. 29, no. 5, pp. 776–788, 2007.

[25] B. Ghadimi and T. Taghikhany, "Dynamic response assessment of an offshore jacket platform with semi-active fuzzy-based controller: a case study," *Ocean Engineering*, vol. 238, Article ID 238109747, 2021.

[26] G. Yan and L. L. Zhou, "Integrated fuzzy logic and genetic algorithms for multi-objective control of structures using MR dampers," *Journal of Sound and Vibration*, vol. 296, no. 1-2, pp. 368–382, 2006.

[27] D. A. Shook, P. N. Roschke, P. Y. Lin, and C. H. Loh, "GA-optimized fuzzy logic control of a large-scale building for seismic loads," *Engineering Structures*, vol. 30, no. 2, pp. 436–449, 2008.

[28] B. Mehrkian, A. Bahar, and A. Chaibakhsh, "Semiactive conceptual fuzzy control of magnetorheological dampers in an irregular base-isolated benchmark building optimized by multi-objective genetic algorithm," *Structural Control and Health Monitoring*, vol. 26, no. 3, p. e2302, 2019.

[29] D. Shook, P. Roschke, and O. Ozbulut, "Superelastic semi-active damping of a base-isolated structure," *Structural Control and Health Monitoring*, vol. 15, no. 5, pp. 746–768, 2008.

[30] H. S. Kim and P. N. Roschke, "Fuzzy control of base-isolation system using multi-objective genetic algorithm," *Computer-Aided Civil and Infrastructure Engineering*, vol. 21, no. 6, pp. 436–449, 2006.

[31] M. E. Uz and M. N. S. Hadi, "Optimal design of semi active control for adjacent buildings connected by MR damper based on integrated fuzzy logic and multi-objective genetic algorithm," *Engineering Structures*, vol. 69, pp. 135–148, 2014.

[32] D. A. Shook, P. N. Roschke, P.-Y. Lin, and C.-H. Loh, "Semi-active control of a torsionally-responsive structure," *Engineering Structures*, vol. 31, no. 1, pp. 57–68, 2009.

[33] M. M. Zafarani, A. M. Halabian, and S. Behbahani, "Optimal coupled and uncoupled fuzzy logic control for magneto-rheological damper-equipped plan-asymmetric structural systems considering structural nonlinearities," *Journal of Vibration and Control*, vol. 24, no. 7, pp. 1364–1390, 2018.

[34] Z. Meng, D. Yang, H. Zhou, and B. P. Wang, "Convergence control of single loop approach for reliability-based design optimization," *Structural and Multidisciplinary Optimization*, vol. 57, no. 3, pp. 1079–1091, 2018.

[35] X. Du and W. Chen, "Sequential optimization and reliability assessment method for efficient probabilistic design," *Journal of Mechanical Design*, vol. 126, no. 2, pp. 225–233, 2004.

[36] N. Kuschel and R. Rackwitz, "Two basic problems in reliability-based structural optimization," *Mathematical Methods of Operations Research*, vol. 46, no. 3, pp. 309–333, 1997.

[37] D. Lee and S. Rahman, "Reliability-based design optimization under dependent random variables by a generalized polynomial chaos expansion," *Structural and Multidisciplinary Optimization*, vol. 65, no. 1, p. 21, 2022.

[38] X. Zeng, Y. Peng, and J. Chen, "Serviceability-based damping optimization of randomly wind-excited high-rise buildings," *The Structural Design of Tall and Special Buildings*, vol. 26, no. 11, Article ID e1371, 2017.

[39] G. Chen, K. Zhang, X. Xue et al., "A radial basis function surrogate model assisted evolutionary algorithm for high-dimensional expensive optimization problems," *Applied Soft Computing*, vol. 116, Article ID 116108353, 2022.

[40] X. Zhang and S. T. Quek, "Efficient subset simulation with active learning Kriging model for low failure probability prediction," *Probabilistic Engineering Mechanics*, vol. 68, Article ID 68103256, 2022.

[41] M. Moustapha and B. Sudret, "Surrogate-assisted reliability-based design optimization: a survey and a unified modular framework," *Structural and Multidisciplinary Optimization*, vol. 60, no. 5, pp. 2157–2176, 2019.

[42] M. Azizi, R. G. Ejlali, S. A. Mousavi Ghasemi, and S. Talatahari, "Upgraded Whale Optimization Algorithm for fuzzy logic based vibration control of nonlinear steel structure," *Engineering Structures*, vol. 192, pp. 53–70, 2019.

[43] K. M. Passino, S. Yurkovich, and M. Reinfrank, *Fuzzy control*, vol. 42, Citeseer, Princeton, NJ, USA, 1998.

[44] P. Pei, Y. Peng, and C. Qiu, "An improved semiactive structural control combining optimized fuzzy controller with inverse modeling technique of MR damper," *Structural and Multidisciplinary Optimization*, vol. 65, no. 9, p. 272, 2022.

[45] P. Pei, Y. Peng, and C. Qiu, "Magnetorheological damper modeling based on a refined constitutive model for MR fluids," *Journal of Intelligent Material Systems and Structures*, vol. 33, no. 10, pp. 1271–1291, 2021.

[46] A. Dounis, P. Tiropanis, G. Syrcos, and D. Tseles, "Evolutionary fuzzy logic control of base-isolated structures in response to earthquake activity," *Structural Control and Health Monitoring*, vol. 14, no. 1, pp. 62–82, 2007.

[47] S. F. Ali and A. Ramaswamy, "Optimal fuzzy logic control for MDOF structural systems using evolutionary algorithms," *Engineering Applications of Artificial Intelligence*, vol. 22, no. 3, pp. 407–419, 2009.

[48] B. Echard, N. Gayton, and M. Lemaire, "AK-MCS: an active learning reliability method combining Kriging and Monte Carlo Simulation," *Structural Safety*, vol. 33, no. 2, pp. 145–154, 2011.

[49] X. Zhang, L. Wang, and J. D. Sørensen, "REIF: a novel active-learning function toward adaptive Kriging surrogate models for structural reliability analysis," *Reliability Engineering and System Safety*, vol. 185, pp. 440–454, 2019.

[50] Y. Shi, Z. Lu, R. He, Y. Zhou, and S. Chen, "A novel learning function based on Kriging for reliability analysis," *Reliability Engineering and System Safety*, vol. 198, Article ID 198106857, 2020.

[51] T. Zhou and Y. Peng, "Reliability analysis using adaptive Polynomial-Chaos Kriging and probability density evolution

method," *Reliability Engineering and System Safety*, vol. 220, Article ID 220108283, 2022.

[52] V. Dubourg, B. Sudret, and J. M. Bourinet, "Reliability-based design optimization using kriging surrogates and subset simulation," *Structural and Multidisciplinary Optimization*, vol. 44, no. 5, pp. 673–690, 2011.

[53] V. Dubourg, *Adaptive Surrogate Models for Reliability Analysis and Reliability-Based Design Optimization*, Université Blaise Pascal-Clermont-Ferrand II, Clermont-Ferrand, France, 2011.

[54] A. K. Chopra, *Dynamics of Structures: Theory and Applications to Earthquake Engineering*, Prentice Hall, Englewood, NJ, USA, 2012.

[55] B. J. Bichon, M. S. Eldred, L. P. Swiler, S. Mahadevan, and J. M. McFarland, "Efficient global reliability analysis for nonlinear implicit performance functions," *AIAA Journal*, vol. 46, no. 10, pp. 2459–2468, 2008.

[56] K. Deb, S. Agrawal, A. Pratap, and T. Meyarivan, "A fast elitist non-dominated sorting genetic algorithm for multi-objective optimization: nsga-II," *Parallel Problem Solving from Nature PPSN VI*, vol. 1917, pp. 849–858, 2000.

[57] China Architecture and Building Press, *50011 G Code for Seismic Design of Buildings, China Academy of Building Research*, China Architecture and Building Press, Beijing, China, 2010.

[58] F. Ma, H. Zhang, A. Bockstedte, G. C. Foliente, and P. Paevere, "Parameter analysis of the differential model of hysteresis," *Journal of Applied Mechanics*, vol. 71, no. 3, pp. 342–349, 2004.

[59] Y. Peng, T. Zhou, and J. Li, "Surrogate modeling immersed probability density evolution method for structural reliability analysis in high dimensions," *Mechanical Systems and Signal Processing*, vol. 152, Article ID 107366, 2021.